Structural plasticity of dendritic secretory compartments during LTP-induced synaptogenesis

Yelena D. Kulik[1, 2], Deborah J. Watson[1, 3], Guan Cao[1],

Masaaki Kuwajima[1], Kristen M. Harris[1*]

1. Center for Learning and Memory
        Department of Neuroscience
        The University of Texas at Austin
        Austin, Texas 78712

2. Current address:
        Yelena Kulik
        Department of Biochemistry and Biophysics
        Kavli Institute for Fundamental Neuroscience
        University of California San Francisco
        San Francisco, CA 94158-0822

3. Current address:
        Deborah J. Watson,
        QPS, LLC
        Pencader Corporate Center
        110 Executive Drive, Suite 7
        Newark, DE 19702

*Corresponding Author:

        Kristen M. Harris, PhD
        The University of Texas at Austin
        Center for Learning and Memory
        1 University Station C7000
        Austin, TX 78712-0805
        kharris@mail.clm.utexas.edu
        512.232.3968

37   **Abstract**

38

39   Long-term potentiation (LTP), an increase in synaptic efficacy following high-frequency

40   stimulation, is widely considered a mechanism of learning. LTP involves local

41   remodeling of dendritic spines and synapses. Smooth endoplasmic reticulum (SER) and

42   endosomal compartments could provide local stores of membrane and proteins,

43   bypassing the distant Golgi apparatus. To test this hypothesis, effects of LTP were

44   compared to control stimulation in rat hippocampal area CA1 at postnatal day 15 (P15).

45   By two hours, small spines lacking SER increased after LTP, whereas large spines did

46   not change in frequency, size, or SER content. Total SER volume decreased after LTP

47   consistent with transfer of membrane to the added spines. Shaft SER remained more

48   abundant in spiny than aspiny dendritic regions, apparently supporting the added

49   spines. Recycling endosomes were elevated specifically in small spines after LTP.

50   These findings suggest local secretory trafficking contributes to LTP-induced

51   synaptogenesis and primes the new spines for future plasticity.

52

53   **Impact Statement**

54   The secretory and recycling components of neuronal dendrites, smooth endoplasmic

55   reticulum and endosomes, were discovered to support synaptogenesis underlying a

56   cellular mechanism of learning and memory in the developing brain.

Introduction

As the longest and most architecturally complex cells in the body, neurons face the unique challenge of regulating membrane and protein levels in distal compartments. Neurons have highly elaborate dendritic arbors. These dendrites possess synapses, points of contact where electrochemical transmission of information occurs. Most of the excitatory synapses are situated on dendritic spines, tiny protrusions with a head and neck comprising a geometry that is essential for shaping electrical signals (Yuste and Denk 1995, Hering and Sheng 2001, Yuste 2011, Harnett, Makara et al. 2012, Harris and Weinberg 2012, Yuste 2013) and providing biochemical compartmentalization (Harris and Stevens 1989, Bourne and Harris 2008, Colgan and Yasuda 2014). For synapses to function appropriately, the levels of receptor proteins at the postsynaptic density must also be finely tuned. Synapses are often located hundreds of micrometers away from the neuronal cell body. Adding to this spatial problem is the challenge of regulating protein abundance on the membrane in a temporally precise manner, as demanded by fast-acting processes such as synaptic potentiation.

Integral membrane proteins destined for the cell surface are canonically thought to be synthesized in the somatic rough endoplasmic reticulum, transported to the Golgi apparatus, and then secreted into the plasma membrane via exocytosis. It is now known that many proteins are translated locally in dendrites, a highly regulated process essential for normal development and plasticity (Sutton and Schuman 2006, Bramham and Wells 2007, Hanus and Schuman 2013). Endoplasmic reticulum (ER) extends into dendrites, forming a continuous tubular network with regions of varying structural complexity and occasional entry into spines (Spacek and Harris 1997, Cooney, Hurlburt et al. 2002, Cui-Wang, Hanus et al. 2012). Together with endosomes, the ER is perfectly positioned to provide a local source of membrane and integral membrane proteins, such as glutamate receptors. However, the Golgi apparatus is absent in most distal dendrites. This puzzling observation has been resolved by recent work demonstrating that dendritic and somatic protein trafficking are highly segregated, and that glutamate receptors are trafficked through a specialized Golgi apparatus-independent pathway from the dendritic ER to the plasma membrane via recycling endosomes (Bowen, Bourke et al. 2017). Structural changes in ER contribute to normal

88   synaptogenesis during development and maturation (Cui-Wang, Hanus et al. 2012).

89   The involvement of this system in activity-induced synaptogenesis is unknown.

90   Long-term potentiation (LTP), the long-lasting enhancement of synaptic strength

91   due to repetitive activity, is thought to underlie learning and memory. This process has

92   been studied extensively in the hippocampus, a key brain region responsible for new

93   memory formation. Insertion of glutamate receptors from an extrasynaptic reserve pool

94   into the postsynaptic compartment is required for LTP in hippocampal area CA1

95   (Granger, Shi et al. 2013). LTP is also accompanied by structural changes in dendritic

96   spines (Bourne and Harris 2012, Bailey, Kandel et al. 2015). In the young rat

97   hippocampus, LTP produces new dendritic spines (Watson, Ostroff et al. 2016),

98   contrasting with adult rat hippocampus where new spine outgrowth is stalled in favor of

99   synapse enlargement (Bourne and Harris 2011, Bell, Bourne et al. 2014). While Golgi

100 apparatus-independent trafficking has not been studied directly in the context of lasting

101 LTP, recycling endosomes (RE) are known to supply AMPA receptors (Park, Penick et

102 al. 2004), and recycling endosome exocytosis is required for spine formation and growth

103 shortly after the induction of LTP (Park, Salgado et al. 2006). Expanded knowledge

104 about the involvement of Golgi apparatus-independent pathways in developmental

105 synaptic plasticity could provide new targets for rescuing dysregulated synaptogenesis

106 in cases of profound developmental disorders (Fiala, Spacek et al. 2002).

107   Here, three-dimensional reconstruction from serial section electron microscopy

108 (3DEM) revealed morphological changes in SER and endosomal compartments 2 hours

109 following the induction of LTP. The findings are consistent with the involvement of the

110 Golgi-bypass secretory system in supporting synaptic plasticity in the developing

111 hippocampus.

112

113 **Results**

114 An acute within-slice experimental protocol (Watson, Ostroff et al. 2016) was used to

115 compare the effects of TBS and control stimulation on subcellular membranous

116 compartments in dendrites. In brief, two stimulating electrodes were positioned ~800 µm

117 apart with a recording electrode halfway in between them in CA1 stratum radiatum of

118 P15 rat hippocampus in one slice from each of two animals (Figure 1A). Baseline

119 responses were collected from both electrodes. TBS was delivered at one stimulating

120 electrode and control stimulation was delivered at the other stimulating electrode,

121 counterbalanced in position relative to CA3 for each experiment. There was a significant

122 increase in the field excitatory postsynaptic potential (fEPSP) slope immediately after

123 TBS (Figure 1B,C). Slices were fixed 120 minutes later. EM image volumes were

124 collected from tissue on a diagonal ~120 µm below and to the side of each stimulating

125 electrode. Segments of spiny dendrites, synapses, and all subcellular membrane

126 compartments were reconstructed in three dimensions (see Methods for details).

127

128 **Figure 1: Within-slice experimental design and electrophysiological outcome.**

129 **(A)** Illustration of an acute slice from a P15 rat hippocampus with a recording electrode

130 (rec.) in the middle of CA1 stratum radiatum between two bipolar stimulating electrodes

131 (S1 and S2). S1 and S2 are separated by 600-800 µm. The two experiments were

132 counterbalanced for which of the two electrodes delivered TBS or control stimulation.

133 Tissue samples collected for 3DEM were located ~120 µm beneath and to the side of

134 the stimulating electrodes. D.G., dentate gyrus; Sub., subiculum. **(B)** Representative

135 waveforms from control (CON, blue) and TBS (LTP, red) sites. Each waveform is the

136 average of the final 10 responses to each stimulating electrode obtained for the last 20

137 min before delivery of TBS at *time 0* (light color) and for 20 minutes before the end of

138 the experiment at 120 min after TBS (dark color). The stimulus intensity was set at

139 population spike threshold to activate a large fraction of the axons in the field of each

140 stimulating electrode. The positive deflection in the post-TBS waveform at ~3-4 ms

141 reflects synchronous firing of pyramidal cells with LTP. **(C)** Changes in the slope of the

142 field excitatory postsynaptic potential (fEPSP), expressed as a percentage of the

143 average baseline response to test-pulses, were recorded for 20 min before delivery of

144 TBS at *time 0* (red) or control stimulation (blue). Responses were recorded for n=2

145 slices for 120 min after the first TBS train, then fixed and processed for 3DEM as

146 described in Methods. Error bars are SEM. Adapted from (Watson, Ostroff et al. 2016)

147 where it was originally published under a CC BY-NC-ND 4.0 license

148 https://creativecommons.org/licenses/by-nc-nd/4.0/).

149　**Figure 1–Source Data 1:** Excel spreadsheet containing the raw numbers that

150　generated the graphs and waveforms for these experiments.

151

152　***Limited entry of SER into dendritic spines***

153　　　　Consistent with previous reports on hippocampal dendrites (Spacek and Harris

154　1997, Cooney, Hurlburt et al. 2002), the SER formed an anastomosing network

155　throughout the dendritic shaft with occasional entry into a subset of dendritic spines

156　(Figure 2A; see Figure 2 - figure supplement 1 for all analyzed dendrites reconstructed

157　with SER). While the dendritic spine density more than doubled 2 hours following TBS,

158　a similar increase in the occurrence of SER in spines did not occur (Figure 2B,C).

159　　　　Spines with small synapses, as measured by the surface area of the

160　postsynaptic density (PSD) (<0.05 μm^2), accounted for the LTP-induced increase in

161　spine density (Figure 2B). This difference was not present at earlier times, and the small

162　spines more than tripled in density by 2 hours post induction of LTP, suggesting that

163　most of this population comprised newly formed spines (Watson, Ostroff et al. 2016).

164　There were no significant effects on SER content in these small spines; not in frequency

165　of spine-localized SER (Figure 2D), average SER volume (Figure 2E), nor average SER

166　surface area (Figure 2F). Since the occurrence of SER did not keep pace with the

167　increase in small spines, the most parsimonious interpretation is that the LTP-induced

168　new spines did not acquire SER.

169　　　　In contrast, while the incidence of SER entry into spines with larger synapses

170　(PSD area ≥ 0.05 μm^2) did not change (Figure 2G), there was however a decrease in

171　the average volume (Figure 2H) and surface area (Figure 2I) of SER in these spines.

172　The spine apparatus is an organelle comprising cisterns of SER laminated with electron

173　dense plates that may serve Golgi functions in spines (Gray 1959, Spacek 1985, Pierce,

174　Mayer et al. 2001). Consistent with previous observations (Spacek and Harris 1997,

175　Cooney, Hurlburt et al. 2002), the spine apparatus appeared in only one dendrite in

176　each condition (data not shown), suggesting that this structure is not central to the

177　activity-induced spinogenesis at this age. Overall, these results reveal that SER entry

178　into dendritic spines is limited and does not scale up with rapid synaptogenesis

179　following LTP at P15.

180

Figure 2: The limited occupancy of spines by SER does not increase during spinogenesis in the LTP condition.

(A) Sample serial section EMs (left) and representative 3D reconstructions of dendrites (right) from control (top) and LTP (bottom) conditions, illustrating dendrites (yellow), SER (green), and synapses (red). Synaptic area was measured as the total surface area of the PSD. Arrows point to SER-containing spines. **(B)** Spine density (#/μm) binned for PSD area. Significant increase in spines following TBS was carried by spines in the category with the smallest PSD areas (<0.05 μm^2; ANOVA $F_{(1,12)}$=50.707, P=0.00001, η^2=0.81). No statistically significant changes occurred in the frequency of spines with larger synapses (PSD area 0.05 to 0.1 μm^2, ANOVA $F_{(1,12)}$=1.079, P=0.31941; PSD area 0.1 to 0.15 μm^2, ANOVA $F_{(1,12)}$=0.09638, P=0.76154; PSD area 0.15 to 0.2 μm^2, ANOVA $F_{(1,12)}$=3.5065, P=0.08569; PSD area >0.2 μm^2, ANOVA $F_{(1,11)}$=3.0778, P=0.10484). Control n=8, LTP n=8 dendrites. **(C)** Decrease in percentage of spines containing SER following TBS (ANOVA $F_{(1,12)}$=10.599, P=.00688, η^2=0.87). Control n=8, LTP n=8 dendrites. **(D-F)** SER content for spines with PSD areas less than 0.05 μm^2. (D) No statistically significant difference between control and LTP conditions in density of spines with SER (ANOVA $F_{(1,12)}$=2.59, P=.13322). Control n=8, LTP n=8 dendrites. (E) No statistically significant difference in average SER volume per SER-containing spine between control and LTP conditions (hnANOVA $F_{(1,14)}$=.73111, P=.40692). Control n=12, LTP n=15 spines. (F) No statistically significant difference in SER surface area per SER-containing spine between control and LTP conditions (hnANOVA $F_{(1,14)}$=3.3120, P=0.09022). Control n=12, LTP n=15 spines. **(G-I)** SER content for spines with total PSD area equal to or greater than 0.05 μm^2. (G) No statistically significant difference in density of spines with SER between control and LTP conditions (ANOVA $F_{(1,12)}$=2.1641, P=0.16700). Control n=8, LTP n=8 dendrites. (H) Reduction in average SER volume per SER-containing spine in the LTP relative to control condition (hnANOVA $F_{(1,38)}$=5.7205, P=0.02182, η^2=0.13). Control n=29, LTP n=25 spines. (I) Reduction in average SER surface area in SER-containing spines in the LTP relative to control condition (hnANOVA $F_{(1, 38)}$=4.5873 P=0.03868, η^2=0.12).

210 Control n=29, LTP n=25 spines. Bar graphs show mean ± S.E.M. Control (CON, blue)

211 and TBS (LTP, red).

212 **Figure 2 – figure supplement 1:** All analyzed dendrites fully reconstructed with SER,

213 aligned left to right from least to greatest spine density. Scale cube is 0.5 µm on each

214 side.

215 **Figure 2–Source Data 1:** Excel spreadsheets containing the raw numbers that

216 generated the graphs in each part of this figure along with the summary of statistics.

217 *Reduced complexity in shaft SER after LTP*

218 Previous work demonstrated in cultured neurons that local zones of ER

219 complexity produce ER exit sites and compartmentalize membrane proteins near the

220 base of dendritic spines (Cui-Wang, Hanus et al. 2012). Consistent with this finding,

221 SER was inhomogeneously distributed across spiny and aspiny regions of the dendrites

222 in both control and LTP conditions. SER appeared as small circular profiles on some

223 sections, and swollen cisternae with bridging elements on other sections (Figure 3A). In

224 3D reconstruction, the primarily tubular structure of SER in aspiny regions and the

225 expanded SER in spiny regions of the dendrite become apparent (Figure 3B). Following

226 LTP, there was a trend towards reduced shaft SER surface area (Figure 3C) that

227 reached statistical significance with reduced shaft SER volume (Figure 3D) when

228 quantified across the total length of the dendritic segments. The SER complexity was

229 estimated by summing the dendritic shaft SER cross-sectional areas in each section,

230 assigning the value to the spiny or aspiny segments, and summing across their

231 independent lengths (Cui-Wang, Hanus et al. 2012). This measure of SER complexity

232 was greater in spiny than aspiny segments under both conditions yet was significantly

233 reduced in both the aspiny and spiny regions following LTP relative to the control

234 condition (Figure 3E). Considering the prior work, this outcome suggests that SER

235 resources may have contributed to the spine outgrowth by 2 hours following the

236 induction of LTP.

237

238 **Figure 3: Reduction in shaft SER following LTP.**

239 **(A)** Electron micrographs showing the dendrite (yellow), SER (green), and synapses

240 (red). For both control and LTP, the SER in the aspiny segments forms small cross-

241 sectioned tubules, whereas in the spiny segments the SER tubules are broadly

242 expanded. **(B)** Sample 3D reconstructions from serial section electron micrographs of

243 SER-containing dendrites, illustrating spiny segments (yellow) and aspiny segments

244 (blue) while the other colors match Figure 2. Aspiny segments consist of two or more

245 sections (>100 nm) of no spine origins. Spiny segments had at least one spine and

246 were surrounded by aspiny segments. Scale cube is 0.5 µm on each side. **(C)** No

247 statistically significant differences between control and LTP conditions were found in

248 surface area of SER in the dendritic shaft (ANOVA $F_{(1,12)}$=3.8833, P=0.07228). Control

249 n=8, LTP n=8 dendrites. **(D)** Volume of dendritic SER network was reduced in the LTP

250 relative to control conditions (ANOVA $F_{(1,12)}$=6.4397, P=0.02605, η^2=0.35). Control n=8,

251 LTP n=8 dendrites. **(E)** Summed cross-sectional area of SER tubules and cisterns as a

252 measure of changes in complexity. More SER on spiny than aspiny sections within both

253 control (hnANOVA $F_{(1,1432)}$=51.672, P<0.00000, η^2=0.034; spiny n=493, aspiny n=955

254 sections) and LTP conditions (hnANOVA $F_{(1,324)}$=17.535, P=0.00003, η^2=0.013; spiny

255 n=714, aspiny n=626 sections). Reduced SER complexity with LTP for both spiny

256 (hnANOVA $F_{(1,1191)}$=51.745, P<0.00000, η^2=0.019; Control n=493, LTP n=714 sections)

257 and aspiny sections (hnANOVA $F_{(1,1565)}$=29.991, P<0.00000, η^2=0.042; Control n=955,

258 LTP n=626 sections) relative to control. Bar graphs show mean ± S.E.M. Control (CON,

259 blue) and TBS (LTP, red).

260 **Figure 3–Source Data 1:** Excel spreadsheets containing the raw numbers that

261 generated the graphs in each part of this figure along with the summary of statistics.

262

263 ***Identifying the dendritic trafficking network***

264 Recent work has shown that SER participates in a local, Golgi apparatus-

265 independent secretory trafficking pathway through recycling endosomes in dendrites

266 (Bowen, Bourke et al. 2017). Recycling endosomes have been identified as transferrin

267 receptor-positive membrane compartments in dendrites by immuno-EM (Park, Salgado

268 et al. 2006). Other work found that non-SER subcellular components endocytose BSA-

269 conjugated gold particles from the extracellular space (Cooney, Hurlburt et al. 2002).

270 Together these findings suggest that while these two compartments interact, the SER is

271   not an endocytic structure. Here we considered the possibility that the endosome-based

272   satellite system was also mobilized during LTP.

273   Once the continuous network of SER was reconstructed, the non-SER

274   compartments could be identified as distinct terminating structures. Endosomal

275   subtypes were classified as depicted in Figure 4A (Cooney, Hurlburt et al. 2002, Park,

276   Salgado et al. 2006, Deretic 2008, von Bartheld and Altick 2011). Coated pits, coated

277   vesicles, and large vesicles were treated as one category of primary endocytic

278   structures. Sorting complexes and recycling complexes were treated as functionally

279   separate categories. Whorls, free multivesicular bodies, lysosomes, and

280   autophagosomes were classified as degradative structures. Detailed descriptions based

281   on EM morphology follow.

282   Tubules were cylindrical in shape with a smooth outer membrane, uniform

283   diameter, and a dark, grainy interior. When two or more tubules occurred in proximity,

284   they were categorized as a recycling complex (Figure 4B; Figure 4–figure supplement 1,

285   Figure 4–video 1). Vesicles were distinguished from tubules by examining adjacent

286   sections. Small vesicles (40-60 nm diameter, Figure 4B; Figure 4–figure supplement 1)

287   and large vesicles (60-95 nm diameter) had a smooth outer membrane and ended

288   within 1-2 sections. Coated pits were omega-shaped invaginations surrounded by

289   clathrin coats (Figure 4C; Figure 4–figure supplement 2). Coated vesicles had a clathrin

290   coat, were free-floating in the cytoplasm. Occasionally, clathrin-coated buds were

291   observed on the ends of tubules.

292   Multivesicular bodies (MVB) contained a variable number of internal vesicles.

293   When a multivesicular body was found surrounded by tubules, the grouping was

294   categorized as a sorting complex (Figure 4D; Figure 4–figure supplement 3 and figure

295   4-video 2). Future work might reveal some MVBs to be exosomal compartments

296   (Ashley, Cordy et al. 2018, Pastuzyn, Day et al. 2018). Amorphous vesicles had a

297   smooth membrane, an electron-lucent interior, and an irregular shape (Figure 4E;

298   Figure 4–figure supplement 4).

299   Lysosomes were spherical structures with a homogeneous, electron-dense

300   interior enclosed by one membrane and measuring 70-150 nm in diameter (Figure 4F;

301   Figure 4 – figure supplement 5). Lysosomes were classified as degradative structures.

302   A MVB was considered to be a primary lysosome, namely a degradative structure,

303   when found alone and containing vesicles or pieces of membrane in a dark matrix

304   (Parton, Simons et al. 1992, Futter, Pearse et al. 1996, Mukherjee, Ghosh et al. 1997,

305   Cooney, Hurlburt et al. 2002). Whorls had multiple convoluted membranes spanning

306   many sections, had a single point of entry into the dendrite, and were classified as

307   degradative structures (Figure 4G; Figure 4– figure supplement 6; Figure 4 –video 3).

308   All non-degradative structures were classified as constructive for the quantitative

309   analyses presented next.

310

311   **Figure 4: Identification of endosomal compartments.**

312   **(A)** Model of the dendritic endosomal pathway. Clathrin-coated pits (CPs) invaginate,

313   becoming clathrin-coated vesicles (CVs) and large vesicles (LVs) after coat shedding.

314   Large vesicles fuse to form tubules, recycling complexes (RCs), and sorting complexes

315   (SCs) with a multivesicular body (MVB). From here, the sorted material may be sent to

316   the plasma membrane via small vesicles (SVs) that pinch off coated tips of tubules.

317   MVBs may serve as exosomes (Exo) or primary lysosomes, that are more darkly

318   stained than exosomes due to the acidic cytomatrix of lysosomes. (Adapted from

319   Cooney, Hurlburt et al., 2002). Sample electron micrographs illustrate **(B)** recycling

320   complex (pink arrow) and small vesicles (purple arrow), **(C)** clathrin-coated pit (orange

321   arrow), **(D)** sorting complex (light blue arrows point to multivesicular body (MVB) in the

322   center and tubules around it), **(E)** amorphous vesicle (green arrow), **(F)** lysosome (black

323   arrow), and **(G)** whorl (black arrow). Scale bar in (G) is 0.5 µm for all images.

324   *Figure 4 – figure supplement 1:* Sample images from the LTP condition of dendritic

325   (yellow) recycling complex with multiple tubules (pink) entering the spine neck, and two

326   small vesicles (purple arrow) in a different dendritic spine. D28 FZYJV sections 108-

327   111. Scale bar 0.5 µm.

328   *Figure 4 – Video 1:* Video paging through dendritic from the LTP condition including

329   sections 96-121 of D28 FZYJV.

330   *Figure 4 – figure supplement 2:* Sample images of coated pit (orange) inside the

331   dendritic shaft (yellow) from a dendrite in the LTP condition, D25 DCPBM sections 121-

332   124. Scale bar 0.5 µm

333   *Figure 4 – figure supplement 3:* Sample images of sorting complex (turquoise) inside

334   the dendritic shaft from the control condition, with one tubule entering a spine neck

335   (right side row 3). D26 PWCNZ sections 41-44. Scale bar 0.5 µm.

336   *Figure 4 – video 2*: A sorting complex (turquoise) in a dendrite (yellow) from the control

337   condition is D26 PWCNZ and includes sections 35-46.

338   **Figure 4 – figure supplement 4:** Sample image of an amorphous vesicle in the

339   dendritic shaft of the LTP condition from D35 DCPBM sections 25-28. Scale bar 0.5 µm.

340   **Figure 4 – figure supplement 5:** Sample images of degradative lysosome (black) in

341   the dendritic shaft (yellow) of the LTP condition from D17 FZYJV sections 146-149*.*

342   Scale bar 0.5 µm.

343   **Figure 4 – figure supplement 6:** Sample images of degradative whorl (black) in a

344   dendrite (yellow) of the control condition from D69 FXBVK sections 176-180. Scale bar

345   0.5 µm

346   **Figure 4 – video 3:** A degradative whorl (black) in a dendrite of the control condition

347   from D69 FXBVK sections 170-187.

348   **Figure 4–Source Data 1:** Excel spreadsheets containing details of the locations of

349   each object in Figure 4.

350

351   ***Constructive endosomes occurred more frequently in spines after LTP***

352   Endosomal structures occurred in the dendritic shafts and a subset of spines

353   (Figure 5A; see Figure 5-figure supplement 1 for all analyzed dendrites reconstructed

354   with constructive endosomes). Overall, endosomal frequency did not change

355   significantly across conditions within dendritic shafts (Figure 5B); however, when

356   analyzed by subtype the occurrence of recycling complexes was increased (Figure 5B).

357   Similarly, there was no significant effect of LTP relative to the control condition on

358   endosomal distribution to aspiny or spiny dendritic segments.

359   In contrast, there was a substantial increase in the occurrence of dendritic spines

360   with endosomes, an effect that was confined to spines with small PSD areas (<0.05

361   µm^2, Figure 5A,C,D). Furthermore, this increase in spines involved constructive

362   endocytic compartments (including coated pits, coated vesicles, large vesicles,

363   recycling complexes, and small vesicles), with no significant effects on the rare

364 occurrence of spines with amorphous vesicles, sorting complexes, or degradative

365 structures (Figure 5E; see Figure 5-figure supplement 2 for all analyzed dendrites

366 reconstructed with degradative endosomes). These data suggest that the non-canonical

367 secretory trafficking contributes locally in support of spines added 2 hours following the

368 induction of LTP at P15.

369

370 **Figure 5: Increased occurrence of endosomes in small spines after LTP.**

371 **(A)** Sample serial EM sections and representative 3D reconstructed dendrites illustrate

372 the distribution of endosomal compartments from control and LTP conditions. Dendrites

373 are yellow, synapses are red, and color-coded arrows point to endosome-containing

374 spines. The color-coded key in the lower left corner indicates amorphous vesicles (AV),

375 recycling complexes (RC), coated pits (CP), coated vesicles (CV), large vesicles (LV),

376 sorting complexes (SC), small vesicles (SV) and degradative structures (DEG); these

377 abbreviations apply also to the graphs. Vesicles are represented as 100nm spheres

378 (AV, CP, CV, LV, and SV). The other structures (RC, SC, DEG) are reconstructed in 3D

379 to scale.

380 **(B)** Endosomal structures in dendritic shafts (#/µm) with relative distributions to aspiny

381 and spiny segments in control (CON) and LTP conditions. Overall, shaft endosomes

382 (hnANOVA $F_{(1,293)}$=0.93104, P=0.33539), degradative structures (hnANOVA

383 $F_{(1,293)}$=0.47789, P=0.48993) or constructive endosomal compartments (Constr. = all

384 minus degradative; hnANOVA $F_{(1,293)}$=0.62167, P=0.43107) did not differ between LTP

385 and control conditions or segment locations. Recycling complexes (RC) were greater in

386 the LTP than control dendritic shafts (hnANOVA $F_{(1,293)}$=6.4920, P=0.01135, η^2=0.022),

387 but no significant differences occurred in the other categories: amorphous vesicles

388 (hnANOVA $F_{(1,293)}$=1.5092, P=0.22025); small vesicles (hnANOVA $F_{(1, 293)}$=1.1699,

389 P=28031); coated pits, coated vesicles, and large vesicles (hnANOVA $F_{(1,293)}$=0.89152,

390 P=0.34584); and sorting complexes (hnANOVA $F_{(1,293)}$=0.45286, P=0.50151). (For

391 control (CON) n = 151 aspiny + spiny segments and for LTP n=158 aspiny + spiny

392 segments.) **(C)** More dendritic spines contained endosomes along the dendrites in the

393 LTP than the control condition (ANOVA $F_{(1,12)}$=18.047, P=0.00113, η^2=0.60), an effect

394 that was carried by spines with PSD areas less than 0.05 µm^2 (ANOVA $F_{(1,12)}$=23.642,

395   P=0.00039, η^2=0.66) but not in spines with PSD area $\geq$0.05 µm^2 (ANOVA

396   F$_{(1,12)}$=0.84714, P=0.37550). **(D)** Stability in percentage of spines containing

397   endosomes following TBS (ANOVA F$_{(1,12)}$=.72158, P=.41225). **(E)** Among spines with

398   PSD area less than 0.05 µm^2, the increase in occupancy of endosomes was due to

399   more with coated pits, coated vesicles, and large vesicles (ANOVA F$_{(1,12)}$=4.94433,

400   P=0.046140, η^2=0.29), recycling complexes (ANOVA F$_{(1,12)}$=11.009, P=0.00613,

401   η^2=0.48), and more with small vesicles (ANOVA F$_{(1,12)}$=5.2575, P=0.04072, η^2=0.30).

402   No significant changes in spine occupancy occurred for amorphous vesicles (ANOVA

403   F$_{(1,12)}$=1, P=0.33705), sorting complexes (ANOVA F$_{(1,12)}$=1, P=0.33705), or degradative

404   structures (ANOVA F$_{(1,12)}$=0.46689, P=0.5074). Bar graphs show mean ± S.E.M. (For

405   **C-E**, Control (CON, n=8 full dendrite reconstructions) and LTP (n=8 full dendrite

406   reconstructions).

407   **Figure 5 – figure supplement 1:** All analyzed dendrites fully reconstructed with

408   constructive endosomes, aligned left to right from least to greatest spine density. Scale

409   cube is 0.5 µm on each side.

410   **Figure 5 – figure supplement 2:** All analyzed dendrites fully reconstructed with

411   intracellular degradative structures, aligned left to right from least to greatest spine

412   density. Scale cube is 0.5 µm on each side.

413   **Figure 5–Source Data 1:** Excel spreadsheets containing the raw numbers that

414   generated the graphs in each part of this figure along with the summary of statistics.

415

416   **Discussion**

417   These results provide several advances towards understanding mechanisms of

418   enduring LTP in the developing hippocampus. A population of spines that increased in

419   density by 2 hours after the induction of LTP relative to control stimulation had small

420   synapses and mostly lacked SER. Spines with larger synapses were unchanged in

421   density and retained SER in similar proportions under both conditions. The distribution

422   of SER along the dendritic shaft was non-uniform, with greater abundance and

423   complexity in spiny than aspiny regions under control and LTP conditions. However, the

424   shaft SER was reduced in volume and complexity after LTP. In conjunction, there was

425   an LTP-related increase in endosomal structures confined to the small, presumably

426   newly formed spines. This elevation involved constructive endocytic, recycling, and

427   exocytic structures in the small spines. In contrast, no differences occurred between

428   control and LTP conditions in the frequency or locations of the degradative structures.

429   These data are from two animals using the within-slice paradigm to control for

430   between-slice variance. The stimulating electrodes were positioned such that the

431   sampling of dendrites was counter-balanced with respect to position from the CA3

432   axons that were stimulated. Dendrites were matched for caliber to avoid the confound

433   that thicker dendrites have more spines per micron. Future work will be needed to

434   determine whether these findings generalize beyond the medium caliber dendrites and

435   position within the dendritic arbor, and to other slice and LTP induction paradigms.

436   The findings suggest a model in which local Golgi apparatus-independent

437   secretory trafficking adds and prepares new spines for subsequent plasticity (Figure 6).

438   TBS induces LTP via the insertion of glutamate receptors from recycling endosomes

439   and lateral diffusion (Malinow and Malenka 2002, Choquet and Triller 2013). By 5

440   minutes (early LTP), there is a temporary swelling of spines and recycling endosomes

441   are recruited into the spines; however the PSD is not enlarged at this early timepoint

442   suggesting receptors are inserted into pre-existing slots (Park, Penick et al. 2004,

443   Lisman and Raghavachari 2006, Park, Salgado et al. 2006, Bourne and Harris 2011,

444   MacGillavry, Song et al. 2013, Watson, Ostroff et al. 2016). By two hours (late LTP),

445   shaft SER decreases as it contributes membrane and proteins via ER exit sites to the

446   formation of new spines, which have silent synapses lacking AMPAR. Constructive

447   endosomes are recruited to the new spines and provide a reserve pool of receptors that

448   are in position for rapid insertion of AMPAR upon subsequent potentiation.

449

450   **Figure 6: Model of the contribution of dendritic secretory compartments to LTP-**

451   **induced synaptogenesis.** Smooth endoplasmic reticulum (SER, green), postsynaptic

452   density (PSD, red), small vesicle or recycling endosome (RE, turquoise), new silent

453   spines (orange), control activation (Con), theta-burst stimulation (TBS), long-term

454   potentiation (LTP), AMPA receptors (AMPAR).

455

456   *Effects of LTP on SER and Spines*

457   Previous work has shown that integral membrane proteins rapidly diffuse

458   throughout tubular SER and become confined in regions where the SER is more

459   complex, having branches between tubules and distended cisternae (Cui-Wang, Hanus

460   et al. 2012). As spine density increases across development so too does SER

461   complexity, leading to decreased mobility of ER membrane cargo with age. SER

462   complexity was measured as the summed cross-sectional area to capture the local

463   variation. SER and spine density were positively correlated where more dendritic spines

464   clustered locally. Using the same methods, we found SER volume and complexity were

465   greater in spiny than aspiny regions and were reduced in conjunction with TBS-induced

466   spinogenesis along these P15 dendrites. This result suggests that the membrane lost

467   from SER in the shaft could have been used to build new spines after LTP.

468   In adult hippocampal area CA1, LTP produced synapse enlargement at the

469   expense of new spine outgrowth (Bourne and Harris 2011, Bell, Bourne et al. 2014,

470   Chirillo, Waters et al. 2019). SER is a limited resource, entering only 10-20% of

471   hippocampal dendritic spines (Spacek and Harris 1997, Cooney, Hurlburt et al. 2002,

472   Chirillo, Waters et al. 2019). Spines containing SER are larger than those without SER,

473   and in adults 2 hours after induction of LTP the SER was elaborated into a spine

474   apparatus in spines with enlarged synapses (Chirillo, Waters et al. 2019). Spines

475   clustered around the enlarged spines and local shaft SER remained complex, whereas

476   distant clusters had fewer spines than control dendrites and lost local shaft SER. These

477   findings suggest that mature dendrites support a maximum amount of synaptic input

478   and strengthening of some synapses uses resources that would otherwise be targeted

479   to support spine outgrowth, even in adults.

480   At P15, CA1 dendrites have less than one-third mature synaptic density, which

481   will nearly reach adult levels in another week (Kirov, Goddard et al. 2004). These

482   findings suggest that P15 may well be an age when synaptogenesis predominates over

483   the growth of existing synapses, which may account for the spinogenesis response to

484   LTP. At P15, SER was also restricted to a small number of spines, and like adults the

485   few spines that had SER were larger than those without SER (Chirillo, Waters et al.

486   2019). However, at P15, most of the small, presumably newly formed spines did not

487   contain SER. Similar to adults, shaft SER was reduced in complexity and volume, but at

488   P15 the redistribution was apparently targeted only to the plasma surface, rather than

489   elaboration of the spine apparatus and growth of potentiated spines, as in adults

490   (Chirillo, Waters et al. 2019). These findings suggest that synapse growth occurs where

491   synapses had already been activated or previously potentiated, and few of those

492   existed at P15 prior to the induction of LTP. Thus, resources were available for spine

493   outgrowth to dominate. Future work is needed to learn when the shaft SER recovers,

494   and when this recovery becomes necessary for additional synaptogenesis or synapse

495   enlargement as the animals mature.

496   SER regulates intracellular calcium ion concentration (Verkhratsky 2005).

497   Regulation of postsynaptic calcium levels is necessary for the expression of synaptic

498   plasticity (Lynch, Larson et al. 1983, Malenka, Kauer et al. 1988), hence the presence of

499   SER could be important for signaling cascades associated with LTP and stabilization of

500   AMPA receptors at potentiated synapses (Borgdorff and Choquet 2002). Consistent

501   with this, spines with larger synapses tended to contain SER, and were maintained at

502   stable density post-TBS. However, it might be of some concern that calcium regulation

503   is disrupted by the reduction in SER volume in both adult and P15 hippocampal

504   dendritic shafts by 2 hours after induction of LTP. The reduction in SER volume was by

505   no means complete, and instead likely reflects the multiple roles of SER in membrane

506   and protein trafficking in addition to the regulation of calcium. That a substantial amount

507   of shaft SER remains well after the induction of LTP, supports the hypothesis that SER

508   is a dynamically regulated resource at both ages.

509

510   ***Role of Satellite Secretory System in Synaptogenesis and Subsequent Plasticity***

511   Dendrites support local processing and secretory trafficking of newly synthesized

512   cargo independent of a Golgi apparatus (Bowen, Bourke et al. 2017). Secretory cargo

513   passes from the ER to ER-Golgi intermediate compartments (ERGICs) into recycling

514   endosomes en route to the plasma membrane. While molecular understanding of this

515   pathway has been achieved, the spatial organization of the responsible organelles has

516   been nebulous. Recycling endosomes were seen about 25% of spines on cultured

517   neurons that also contained synaptopodin, a marker for the ER-derived spine apparatus

518   (Bowen, Bourke et al. 2017). This finding suggested that recycling endosomes might

519   receive newly synthesized cargo directly from a spine apparatus. However, at P15, only

520   one spine apparatus was found in each of the control and TBS conditions, suggesting

521   that recycling endosomes derive from alternate recycling organelles in the dendritic

522   shaft. Previously, this satellite secretory system has only been studied in neurons under

523   baseline conditions in culture. Here, we provide the first evidence that this specialized

524   secretory system locally supports spine formation during plasticity.

525   Synaptogenesis at P15 does not precede the expression of LTP, as evidenced

526   by a lack of added spines at 5 minutes following TBS (Watson, Ostroff et al. 2016). The

527   magnitude of potentiation following the initial TBS is constant across time, so the added

528   small spines at 2 hours after the induction of LTP are likely to be functionally silent.

529   Hence, the newly added spines could be viewed as a form of heterosynaptic plasticity

530   that readies the neurons for subsequent potentiation. In support of this hypothesis, a

531   second bout of TBS delivered 90 minutes after the first TBS produces substantial

532   additional potentiation at this age (Cao and Harris 2012). Many of the added small

533   spines contained endosomes at 2 hours after the initial induction of LTP. These

534   endosomes might be interpreted as a heterosynaptic mechanism for long-term

535   depression, namely internalizing receptors from pre-existing spines. However, since

536   most of the endosomal structures occupied the added small spines and were of a

537   constructive nature, they could instead be available to convert the new silent synapses

538   to active synapses after a later bout of potentiation. Such a mechanism would support

539   the establishment of functional circuits as the young animals learn and begin to form

540   memories.

541

542   **Methods and Materials**

KEY RESOURCES TABLE

Reagent type (species) or resource	Designation	Source or Reference	Identifiers	Additional Information

Strain, strain background (Rattus norvegicus, male)	Long-Evans Rat	Charles River	Charles River strain# 006; RRID:RGD_ 2308852	
Chemical compound, drug	Potassium ferrocyanide	Sigma-Aldrich	Cat# P3289	
Chemical compound, drug	Osmium tetroxide	Electron Microscopy Sciences	Cat# 19190	
Chemical compound, drug	Uranyl acetate	Electron Microscopy Sciences	Cat# 22400	
Chemical compound, drug	LX-112 embedding kit	Ladd Research Industries	Cat# 21210	
Chemical compound, drug	Lead nitrate	Ladd Research Industries	Cat# 23603	
Chemical compound, drug	Pioloform F	Ted Pella	Cat# 19244	
Software, algorithm	Igor Pro 4	WaveMetrics	https://www. wavemetrics. net/	
Software, algorithm	Reconstruct	Fiala 2005	Executable and manual: http://synaps eweb.clm.ut exas.edu/sof tware-0	Source at: https://gith ub.com/org s/Synapse Web/teams /reconstruc t- developers
Software, algorithm	STATISTICA 13 Academic	Tibco	https://onthe hub.com//sta tistica/	
Other	Tissue slicer	Stoelting	Cat # 51425	
Other	Vibratome	Leica Biosystems	VT1000S	

Other	Ultramicrotome	Leica Biosystems	UC6	Used with a Diatome Ultra35 knife
Other	SynapTek Grids	Ted Pella	Cat# 4514 or 4516	
Other	Diffraction grating replica	Electron Microscopy Sciences	Cat# 80051	
Other	Transmission electron microscope	JEOL	JEM-1230	
Other	Harris Lab wiki	Harris Lab	https://wikis.utexas.edu/display/khlab/	This wiki site hosts experimental methods used for this paper and updates.

543

Animals

545   Hippocampal slices (400 µm) were rapidly prepared from P15 male Long-Evans rats

546   (RRID:RGD_2308852, n > 100, including the initial test experiments and slices used in

547   prior work for the 5-minute and 30-minute time points (Watson, Ostroff et al. 2016)). For

548   the 2-hour time point reported here, one slice each from 2 rats met the strict physiology

549   and ultrastructural criteria for inclusion as outlined below. All procedures were approved

550   by the University of Texas at Austin Institutional Animal Care and Use Committee and

551   were followed in compliance with NIH requirements for humane animal care and use

552   (Protocol number 06062801). All rats were of comparable features indicative of health at

553   the time they were taken for experimentation.

554

Preparation and recording from acute hippocampal slices

556   Rats were decapitated and the left hippocampus was removed and sliced into 400 µm

557   thick slices from the middle third of the hippocampus at a 70° traverse to the long axis

558   using a tissue chopper (Stoelting, Wood Dale, IL). Hippocampal slices were kept room

559   temperature (~25°C) in artificial cerebrospinal fluid (ACSF) bubbled with 95% O_2/5%

560   CO_2 (Bourne, Kirov et al. 2007). ACSF consisted of 116.4 mM NaCl, 5.4 mM KCl, 3.2

561   mM $CaCl_2$, 1.6 mM $MgSO_4$, 26.2 $NaHCO_3$, 1.0 mM NaH_2PO_4, and 10 mM D-glucose at

562   pH 7.4. Slices were immediately transferred to nets on top of wells containing ACSF at

563   the interface of humidified O_2 (95%) and CO_2 (5%). Dissection and slice preparation

564   took less than 5 min. The slices were kept at 32°C for approximately 3 hours in vitro

565   prior to recording (Fiala, Kirov et al. 2003). Two concentric bipolar stimulating electrodes

566   (100 µm diameter, Fred Haer, Brunswick, ME) were positioned ~300-400 µm on either

567   side of a single glass extracellular recording electrode in the middle of stratum radiatum

568   for independent activation of subpopulations of synapses (Sorra and Harris 1998,

569   Ostroff, Fiala et al. 2002, Bourne and Harris 2011). The recording electrode was a glass

570   micropipette filled with 120 µM NaCl. After initial recovery period, stable baseline

571   recordings were obtained from both sites for a minimum of 40 min. Extracellular field

572   potentials (fEPSPs) were obtained with custom designed stimulation data acquisition

573   protocols using Igor software (WaveMetrics, Lake Oswego, OR). fEPSPs were

574   estimated by linear regression over 400 µs along maximal initial slope (mV/ms) of test

575   pulses of 100 µs constant, biphasic current. Stimulus intensity was set to evoke 1/2

576   maximum fEPSP slope based on a stimulus/response curve for each experiment and

577   was held constant for the duration of the experiment.

578

579   ***TBS-LTP paradigm***

580   Theta burst stimulation (TBS) was used to induce LTP. TBS was administered by one

581   stimulating electrode as one episode of eight trains 30 seconds apart, each train

582   consisting of 10 bursts at 5Hz of 4 pulses at 100Hz. The control stimulating electrode

583   delivered one pulse every 2 minutes. Stimulations were alternated between the TBS-

584   LTP and the control electrode once every two minutes with a 30 second interval

585   between electrodes. In order to counterbalance across experiments, control and TBS-

586   LTP electrode positions were interchanged between the CA3 and subicular side of the

587   recording electrode (Figure 1A). Physiological responses were monitored for 120 min

588   after the first train of TBS (Figure 1B,C) and then rapidly fixed, as described below.

589

Fixation and processing for 3DEM

590   One slice from each animal was fixed and processed for electron microscopy 2 hours

591   after induction of LTP. Only slices with good physiology were used, defined as a

592   gradually inclining I/O curve in response to incremental increases in stimulus intensity

593   for both stimulating electrodes, a stable baseline response at both stimulating

594   electrodes unchanged at the control site post LTP-induction, and a significant increase

595   in fEPSP slope that was immediately induced by TBS and was sustained for the

596   duration of the experiment. Within a few seconds of the experiment's end, electrodes

597   were removed and slices were immersed in fixative (6% glutaraldehyde and 2%

598   paraformaldehyde in 100 mM cacodylate buffer with 2 mM $CaCl_2$ and 4 mM $MgSO_4$),

599   microwaved at full power (700 W microwave oven) for 10 seconds to enhance

600   penetration of fixative (Jensen and Harris 1989), stored in the fixative overnight at room

601   temperature, rinsed three times for 10 minutes in 100 mM cacodylate buffer, and

602   embedded in 7% low melting temperature agarose. They were then trimmed, leaving

603   only the CA1 region that contained the two stimulating electrodes. They were mounted

604   in agarose and vibra-sliced into 70 µm thick slices (VT1000S, Leica, Nusslock,

605   Germany). Vibra-slices were kept in a 24-well tissue culture dish and examined under a

606   dissecting microscope to locate the vibra-slices containing indentations from the

607   stimulating electrodes.

608   The vibra-slices with the indentations due to the stimulating electrodes and two

609   vibra-slices on either side of these indentations were collected and processed in 1%

610   OsO_4 and 1.5% potassium ferrocyanide in 0.1M cacodylate buffer for 5-10 minutes,

611   rinsed five times in buffer, immersed in 1% OsO_4 and microwaved (1 min on, 1 min off,

612   1 min on) twice with cooling to 20°C in between, and rinsed five times in buffer for two

613   minutes and then twice in water. They were then dehydrated in ascending

614   concentrations of ethanol (50%, 70%, 90%, and 100%) with 1-1.5% uranyl acetate and

615   microwaved for 40 s at each concentration. Finally, slices were transferred through

616   room temperature propylene oxide, embedded in LX-112 (Ladd Research, Williston,

617   VT), and cured for 48 hours at 60°C in an oven (Harris, Perry et al. 2006).

618   Slices with high-quality preservation, defined as dendrites with evenly spaced

619   microtubules, well-defined mitochondrial cristae, and well-defined PSDs that were not

621 thickened or displaced from the membrane, were selected for analysis. The region of

622 interest was selected from middle of the CA1 stratum radiatum and 120-150 μm

623 beneath the air surface, then cut into 150-200 serial sections. The sections were

624 mounted on Pioloform-coated slot grids (Synaptek, Ted Pella, Redding, CA). The

625 sections were counterstained with saturated ethanolic uranyl acetate, then Reynolds

626 lead citrate (Reynolds 1963) for five minutes each, and then imaged with a JEOL JEM-

627 1230 transmission electron microscope with a Gatan digital camera at 5000X

628 magnification along with a diffraction grating replica for later calibration (0.463 μm cross

629 line EMS, Hatfield, PA or Ted Pella). Imaging was conducted blind to condition.

630

631 ***3D reconstructions and measurements of dendrites***

632 A random five-letter code was assigned to each series of images for the experimenter to

633 be blind to the original experimental conditions during data collection. Reconstruct

634 software (freely available at http://www.synapseweb.clm.utexas.edu; (Fiala 2005)) was

635 used to calibrate pixel size and section thickness, align sections, and trace dendrites,

636 SER, endosomes, and PSD. The diffraction grating replica imaged with each series was

637 used to calibrate pixel size. Cylindrical diameters method was used to calculate section

638 thickness (Fiala and Harris 2001). Calculated section thicknesses ranged from 46 to 63

639 nm. Dendrites selected for analysis were chosen based on their orientation (cross-

640 sectioned or radial oblique) and matched for diameter. Microtubule count was used as a

641 measure of dendritic caliber (6-22 MTs) as this range under control condition showed no

642 differences in spine density. All dendrites chosen for the analysis were completely

643 reconstructed. The z-trace tool in Reconstruct was used to measure dendrite lengths

644 across serial sections of each analyzed dendrite. Four dendrites were sampled from

645 each condition (control or TBS-LTP) in each animal, resulting in a total of 16 dendritic

646 segments from four EM series. Each analyzed dendritic segment traversed over 100

647 serial sections. In total, 173 μm of dendritic length was sampled.

648 ***Identification and quantification of subcellular compartments***

649   The process of tracing, reviewing, and curating dendrites, synapses, and

650 subcellular objects was confirmed by three scientists (Kulik, Watson, and Harris) and

651 conducted blind as to condition. On the rare occasions where there was disagreement,

652 we met to arrive at a consensus based on the 3D structures; hence all objects were

653 eventually provided a confirmed identification as outlined below.

654   Dendrites and PSDs were traced and dimensions were quantified as previously

655 described (Watson, Ostroff et al. 2016). SER was identified on the basis of its

656 characteristic morphology of tubules with dark staining membrane, occasional flattened

657 cisternal distensions with a wavy membrane and clear lumen, and continuity across

658 sections within each reconstructed dendrite. Once SER was completely traced, the

659 remaining membrane-bound intracellular compartments were traced and their identity

660 was assigned on the basis of morphology, as described in Results. Criteria used to

661 differentiate endosomes included: 1) <u>Continuity across sections</u>: vesicles appear on

662 single sections; tubules span multiple sections and then terminate; SER is continuous

663 across sections throughout the entire dendrite; MVBs and tubules form a sorting

664 complex when found on continuous sections; 2) <u>Geometry</u>: small and large vesicles are

665 spherical, while amorphous vesicles are not; tubules have a uniform diameter across

666 sections; SER has a highly variable profile across sections; MVBs have an

667 unmistakable outer membrane surrounding multiple internal vesicles, and MVBs have

668 tubules attached when part of a sorting complex; 3) <u>Dimensions</u>: small vesicles are 40-

669 60 nm in diameter; large vesicles are 60-95 nm in diameter; 4) <u>Electron density</u>:

670 amorphous vesicles and SER have a clear lumen; tubules and MVBs have a dark,

671 grainy interior; lysosomes have a very dark, electron-dense interior.

672   Only spines that were entirely contained within the series were used for the

673 analyses of subcellular compartments. In this way, we avoided possible undercounting

674 of compartments that may have entered a portion of an incomplete spine outside the

675 series. Spines were considered to contain a subcellular structure when it entered the

676 head or neck of the spine, but not if it was only at the base of a spine. The frequency of

677 occurrence was calculated as the total number of occurrences of objects divided by the

678 length of dendrite in microns. The 3D visualization of dendrites and subcellular

679 structures was achieved with Reconstruct. The 3D reconstructions from serial EMs

680 allowed us to calculate volumes and surface areas of objects and to assess SER and

681 endosome distribution within dendrites.

682

683   *Statistical analyses*

684   The statistical package STATISTICA (version 13.3; TIBCO, Palo Alto, CA) was used for

685   all analyses. There were two conditions represented in each animal: control (CON), and

686   LTP at 120 min following TBS. In this study, 8 control dendrites (4 from each animal)

687   and 8 LTP dendrites (4 from each animal) were analyzed. One-way ANOVAs were run

688   on all density (#/μm) data involving one measurement per dendrite, in which case

689   n=number of dendrites. Hierarchical nested analysis of variance (hnANOVAs) were run

690   when many measures were obtained from each dendrite (e.g. SER volume per spine,

691   PSD area etc.). In this case, n=total spines, as each spine was considered separately.

692   In hnANOVAs dendrite was nested in condition and experiment, and experiment nested

693   in condition to account for inter-experiment variability. Results of the one-way ANOVAs

694   and hnANOVAs are reported as ($F_{(df\ condition,\ df\ observations)}$ = F value, P value) where df is

695   degrees of freedom presented for condition and error. In hnANOVAs degrees of

696   freedom are further decreased by one for each dendrite. Absolute p values are reported

697   for each test. Statistical tests are reported in the figure legends. Data in bar graphs is

698   plotted as mean ± SEM. Significant P values are indicated by asterisks above the bars.

699   Significance was set at $P < 0.05$. The effect sizes for significant differences are also

700   presented in the figure legends as η^2 (which was determined as $SS_{condition}/SS_{(condition\ +}$

701    $_{error)}$, where SS= sum of squares determined in Statistica for each analysis).

702

703   We have provided the raw images, Reconstruct trace files, and analytical tables in the

704   public domain at Texas Data Repository: DOI: https://doi.org/10.18738/T8/5TX9YA,

705   which is not yet public, but will be upon acceptance of this paper.

706

707   *Caveats*

708   One might be concerned that these data arise from two animals. We note that these

709   experiments are within-slice experiments, namely the control and LTP sites are from

710   independent locations within the same slice from two different animals. Based on

711   numerous preliminary experiments, we found that this approach greatly reduces

712   variation due to slice preparation, in vitro conditions, and subsequent processing for

713   electron microscopy when comparing the control and LTP outcomes. We also note that

714 enhanced statistical power came from the large number of synapses and spines tested

715 using the hierarchical nested ANOVA design with dendrite nested in condition by animal

716 (Figures 2E, F, H, I, 3E). In this way, degrees of freedom are adjusted for animal and

717 dendrites, and outcomes are tested to ensure that no one dendrite or animal carried the

718 findings. In addition, we had power to detect changes using multifactor ANOVAs for

719 measurements that involved one measure per dendrite (#/μm listed on the y axes of

720 Figures 2B-D, 2G, 3C-D, 5B-E). Given the extremely time-consuming nature of the

721 imaging and 3DEM analysis, additional animals and slices were not included.

722

723 **Source Data files (Named "Figure 1-5–Source Data1 in each legend):** There is one

724 source data file for each of figures 1-5 that contains Excel spreadsheets with the object

725 locations in the Reconstruct trace files (provided in the public domain) for EMs. These

726 files also contain the raw numbers that generated graphs in each part of each figure

727 along with the summary of statistics.

728

739

740 **References**

741

742 Ashley, J., B. Cordy, D. Lucia, L. G. Fradkin, V. Budnik and T. Thomson (2018). "Retrovirus-like
743 Gag Protein Arc1 Binds RNA and Traffics across Synaptic Boutons." Cell **172**(1-2): 262-
744 274.e211.

Bailey, C. H., E. R. Kandel and K. M. Harris (2015). "Structural Components of Synaptic Plasticity and Memory Consolidation." Cold Spring Harb Perspect Biol **7**(7): a021758.

Bell, M. E., J. N. Bourne, M. A. Chirillo, J. M. Mendenhall, M. Kuwajima and K. M. Harris (2014). "Dynamics of nascent and active zone ultrastructure as synapses enlarge during long-term potentiation in mature hippocampus." J Comp Neurol **522**(17): 3861-3884.

Borgdorff, A. J. and D. Choquet (2002). "Regulation of AMPA receptor lateral movements." Nature **417**(6889): 649-653.

Bourne, J. N. and K. M. Harris (2008). "Balancing structure and function at hippocampal dendritic spines." Annu. Rev. Neurosci **31**: 47-67.

Bourne, J. N. and K. M. Harris (2011). "Coordination of size and number of excitatory and inhibitory synapses results in a balanced structural plasticity along mature hippocampal CA1 dendrites during LTP." Hippocampus **21**(4): 354-373.

Bourne, J. N. and K. M. Harris (2012). "Nanoscale analysis of structural synaptic plasticity." Curr. Opin. Neurobiol **22**(3): 372-382.

Bourne, J. N., S. A. Kirov, K. E. Sorra and K. M. Harris (2007). "Warmer preparation of hippocampal slices prevents synapse proliferation that might obscure LTP-related structural plasticity." Neuropharmacology **52**(1): 55-59.

Bowen, A. B., A. M. Bourke, B. G. Hiester, C. Hanus and M. J. Kennedy (2017). "Golgi-independent secretory trafficking through recycling endosomes in neuronal dendrites and spines." Elife **6**.

Bramham, C. R. and D. G. Wells (2007). "Dendritic mRNA: transport, translation and function." Nat Rev Neurosci **8**(10): 776-789.

Cao, G. and K. M. Harris (2012). "Developmental Regulation of the Late Phase of Long-Term Potentiation (L-LTP) and Metaplasticity in Hippocampal Area CA1 of the Rat." J Neurophysiol **107**(3): 902-912.

Chirillo, M. A., M. S. Waters, L. F. Lindsey, J. N. Bourne and K. M. Harris (2019). "Local resources of polyribosomes and SER promote synapse enlargement and spine clustering after long-term potentiation in adult rat hippocampus." Sci Rep **9**(1): 3861.

Choquet, D. and A. Triller (2013). "The dynamic synapse." Neuron **80**(3): 691-703.

Colgan, L. A. and R. Yasuda (2014). "Plasticity of dendritic spines: subcompartmentalization of signaling." Annu. Rev. Physiol **76**: 365-385.

Cooney, J. R., J. L. Hurlburt, D. K. Selig, K. M. Harris and J. C. Fiala (2002). "Endosomal compartments serve multiple hippocampal dendritic spines from a widespread rather than a local store of recycling membrane." J. Neurosci **22**(6): 2215-2224.

Cui-Wang, T., C. Hanus, T. Cui, T. Helton, J. Bourne, D. Watson, K. M. Harris and M. D. Ehlers (2012). "Local zones of endoplasmic reticulum complexity confine cargo in neuronal dendrites." Cell **148**(1-2): 309-321.

Deretic, V. (2008). Autophagosome and Phagosome. Autophagosome and Phagosome. V. Deretic. Totowa, NJ, Humana Press**:** 1-10.

Fiala, J. C. (2005). "Reconstruct: a free editor for serial section microscopy." J. Microsc **218**(Pt 1): 52-61.

Fiala, J. C. and K. M. Harris (2001). "Cylindrical diameters method for calibrating section thickness in serial electron microscopy." J. Microsc **202**(Pt 3): 468-472.

Fiala, J. C., S. A. Kirov, M. D. Feinberg, L. J. Petrak, P. George, C. A. Goddard and K. M. Harris (2003). "Timing of neuronal and glial ultrastructure disruption during brain slice preparation and recovery in vitro." J Comp Neurol **465**(1): 90-103.

Fiala, J. C., J. Spacek and K. M. Harris (2002). "Dendritic spine pathology: cause or consequence of neurological disorders?" Brain Res. Brain Res. Rev **39**(1): 29-54.

Futter, C. E., A. Pearse, L. J. Hewlett and C. R. Hopkins (1996). "Multivesicular endosomes containing internalized EGF-EGF receptor complexes mature and then fuse directly with lysosomes." J. Cell Biol. **132**(6): 1011-1023.

796 Granger, A. J., Y. Shi, W. Lu, M. Cerpas and R. A. Nicoll (2013). "LTP requires a reserve pool of
797 glutamate receptors independent of subunit type." Nature **493**(7433): 495-500.
798 Gray, E. G. (1959). "Axo-somatic and axo-dendritic synapses of the cerebral cortex: an electron
799 microscope study." J. Anat **93**: 420-433.
800 Hanus, C. and E. M. Schuman (2013). "Proteostasis in complex dendrites." Nat Rev Neurosci
801 **14**(9): 638-648.
802 Harnett, M. T., J. K. Makara, N. Spruston, W. L. Kath and J. C. Magee (2012). "Synaptic
803 amplification by dendritic spines enhances input cooperativity." Nature **491**(7425): 599-602.
804 Harris, K. M., E. Perry, J. Bourne, M. Feinberg, L. Ostroff and J. Hurlburt (2006). "Uniform serial
805 sectioning for transmission electron microscopy." J. Neurosci **26**(47): 12101-12103.
806 Harris, K. M. and J. K. Stevens (1989). "Dendritic spines of CA1 pyramidal cells in the rat
807 hippocampus: serial electron microscopy with reference to their biophysical characteristics." J.
808 Neurosci **9**(8): 2982-2997.
809 Harris, K. M. and R. J. Weinberg (2012). "Ultrastructure of synapses in the mammalian brain."
810 Cold Spring Harb. Perspect. Biol. **4**(5).
811 Hering, H. and M. Sheng (2001). "Dendritic spines: structure, dynamics and regulation." Nat.
812 Rev. Neurosci **2**(12): 880-888.
813 Jensen, F. E. and K. M. Harris (1989). "Preservation of neuronal ultrastructure in hippocampal
814 slices using rapid microwave-enhanced fixation." J. Neurosci. Methods **29**(3): 217-230.
815 Kirov, S. A., C. A. Goddard and K. M. Harris (2004). "Age-dependence in the homeostatic
816 upregulation of hippocampal dendritic spine number during blocked synaptic transmission."
817 Neuropharmacology **47**(5): 640-648.
818 Lisman, J. and S. Raghavachari (2006). "A unified model of the presynaptic and postsynaptic
819 changes during LTP at CA1 synapses." Sci STKE **2006**(356): re11.
820 Lynch, G., J. Larson, S. Kelso, G. Barrionuevo and F. Schottler (1983). "Intracellular injections
821 of EGTA block induction of hippocampal long-term potentiation." Nature **305**: 719-721.
822 MacGillavry, H. D., Y. Song, S. Raghavachari and T. A. Blanpied (2013). "Nanoscale scaffolding
823 domains within the postsynaptic density concentrate synaptic AMPA receptors." Neuron **78**(4):
824 615-622.
825 Malenka, R. C., J. A. Kauer, R. S. Zucker and R. A. Nicoll (1988). "Postsynaptic calcium is
826 sufficient for potentiation of hippocampal synaptic transmission." Science **242**(4875): 81-84.
827 Malinow, R. and R. C. Malenka (2002). "AMPA receptor trafficking and synaptic plasticity."
828 Annu. Rev. Neurosci **25**: 103-126.
829 Mukherjee, S., R. N. Ghosh and F. R. Maxfield (1997). "Endocytosis." Physiol Rev **77**(3): 759-
830 803.
831 Ostroff, L. E., J. C. Fiala, B. Allwardt and K. M. Harris (2002). "Polyribosomes redistribute from
832 dendritic shafts into spines with enlarged synapses during LTP in developing rat hippocampal
833 slices." Neuron **35**(3): 535-545.
834 Park, M., E. C. Penick, J. G. Edwards, J. A. Kauer and M. D. Ehlers (2004). "Recycling
835 endosomes supply AMPA receptors for LTP." Science **305**(5692): 1972-1975.
836 Park, M., J. M. Salgado, L. Ostroff, T. D. Helton, C. G. Robinson, K. M. Harris and M. D. Ehlers
837 (2006). "Plasticity-induced growth of dendritic spines by exocytic trafficking from recycling
838 endosomes." Neuron **52**(5): 817-830.
839 Parton, R. G., K. Simons and C. G. Dotti (1992). "Axonal and dendritic endocytic pathways in
840 cultured neurons." J. Cell Biol. **119**(1): 123-137.
841 Pastuzyn, E. D., C. E. Day, R. B. Kearns, M. Kyrke-Smith, A. V. Taibi, J. McCormick, N. Yoder,
842 D. M. Belnap, S. Erlendsson, D. R. Morado, J. A. G. Briggs, C. d. Feschotte and J. D. Shepherd
843 (2018). "The Neuronal Gene Arc Encodes a Repurposed Retrotransposon Gag Protein that
844 Mediates Intercellular RNA Transfer." Cell **173**(1): 275.
845 Pierce, J. P., T. Mayer and J. B. McCarthy (2001). "Evidence for a satellite secretory pathway in
846 neuronal dendritic spines." Curr. Biol **11**(5): 351-355.

847   Reynolds, E. S. (1963). "The use of lead citrate at high pH as an electron-opaque stain in
848   electron microscopy." <u>J Cell Biol</u> **17**: 208-212.
849   Sorra, K. E. and K. M. Harris (1998). "Stability in synapse number and size at 2 hr after long-
850   term potentiation in hippocampal area CA1." <u>J. Neurosci</u> **18**(2): 658-671.
851   Spacek, J. (1985). "Three-dimensional analysis of dendritic spines. II. Spine apparatus and
852   other cytoplasmic components." <u>Anat. Embryol. (Berl)</u> **171**(2): 235-243.
853   Spacek, J. and K. M. Harris (1997). "Three-dimensional organization of smooth endoplasmic
854   reticulum in hippocampal CA1 dendrites and dendritic spines of the immature and mature rat." <u>J.</u>
855   <u>Neurosci</u> **17**(1): 190-203.
856   Sutton, M. A. and E. M. Schuman (2006). "Dendritic protein synthesis, synaptic plasticity, and
857   memory." <u>Cell</u> **127**(1): 49-58.
858   Verkhratsky, A. (2005). "Physiology and pathophysiology of the calcium store in the
859   endoplasmic reticulum of neurons." <u>Physiol Rev</u> **85**(1): 201-279.
860   von Bartheld, C. S. and A. L. Altick (2011). "Multivesicular bodies in neurons: distribution,
861   protein content, and trafficking functions." <u>Prog. Neurobiol</u> **93**(3): 313-340.
862   Watson, D. J., L. Ostroff, G. Cao, P. H. Parker, H. Smith and K. M. Harris (2016). "LTP
863   enhances synaptogenesis in the developing hippocampus." <u>Hippocampus</u> **26**(5): 560-576.
864   Yuste, R. (2011). "Dendritic spines and distributed circuits." <u>Neuron</u> **71**(5): 772-781.
865   Yuste, R. (2013). "Electrical compartmentalization in dendritic spines." <u>Annu. Rev. Neurosci</u> **36**:
866   429-449.
867   Yuste, R. and W. Denk (1995). "Dendritic spines as basic functional units of neuronal
868   integration." <u>Nature</u> **375**(6533): 682-684.
869

870

A

S1   rec.   S2

CA1

CA3   D.G.   Sub.

B

CON

LTP

5mV

5ms

C

Figure 1

A CON

LTP

0.5 μm

0.5 μm

1 μm³

B

Sp / μm

***

CON +SER
CON -SER
LTP +SER
LTP -SER

PSD Area (μm²)
.05 .10 .15 .20 >.20

C

% +SER Sp

**

D +SER Sp / μm

E Sp SER Vol (μm³)

F Sp SER Surf (μm²)

PSD Area < 0.05 (μm²)

G +SER Sp / μm

H Sp SER Vol (μm³)

*

I Sp SER Surf (μm²)

*

PSD Area ≥ 0.05 (μm²)
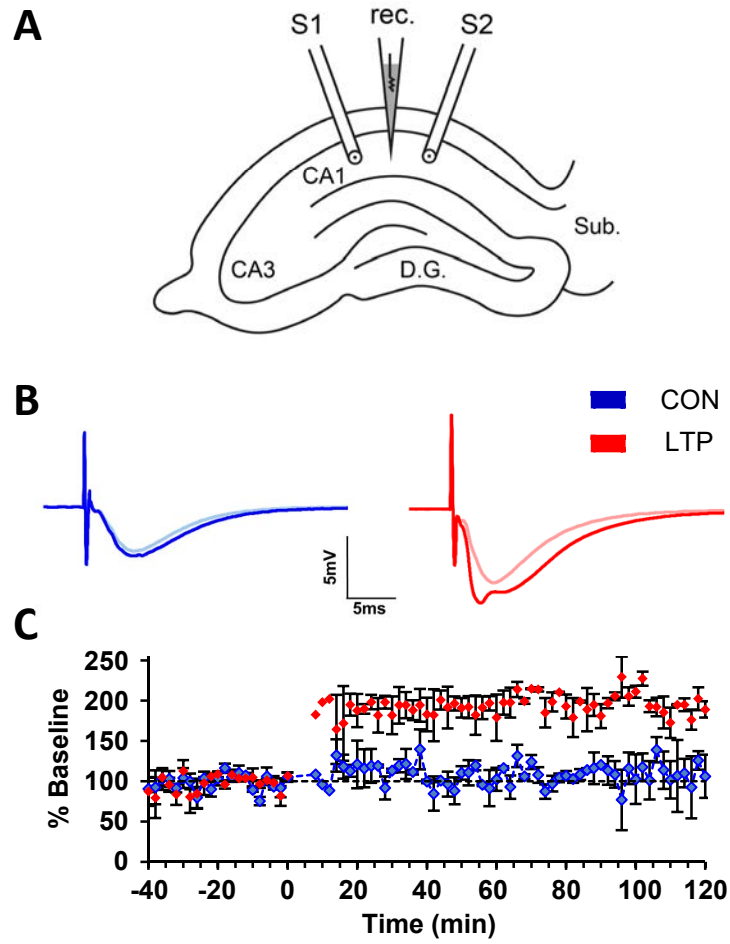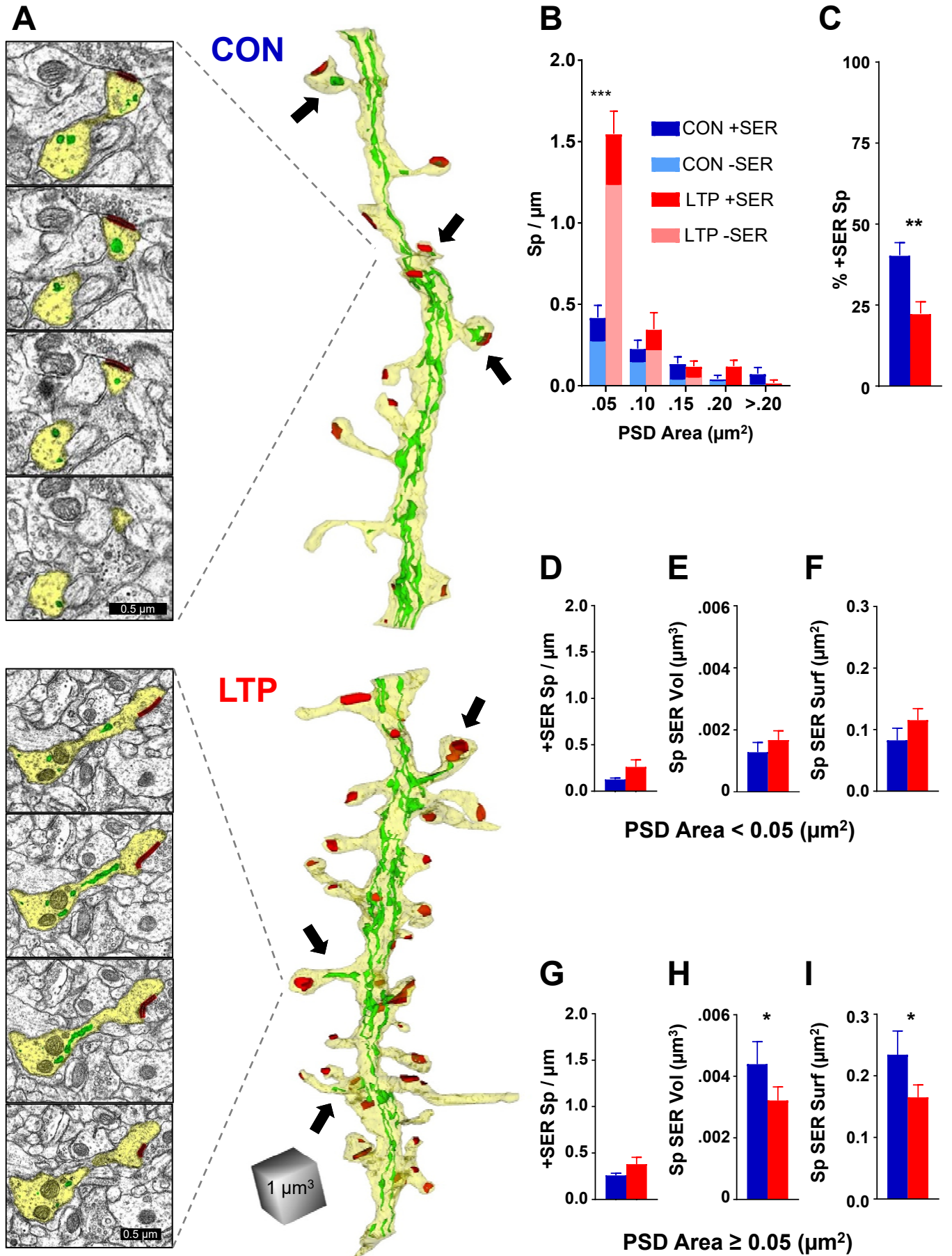
Figure 2

CON
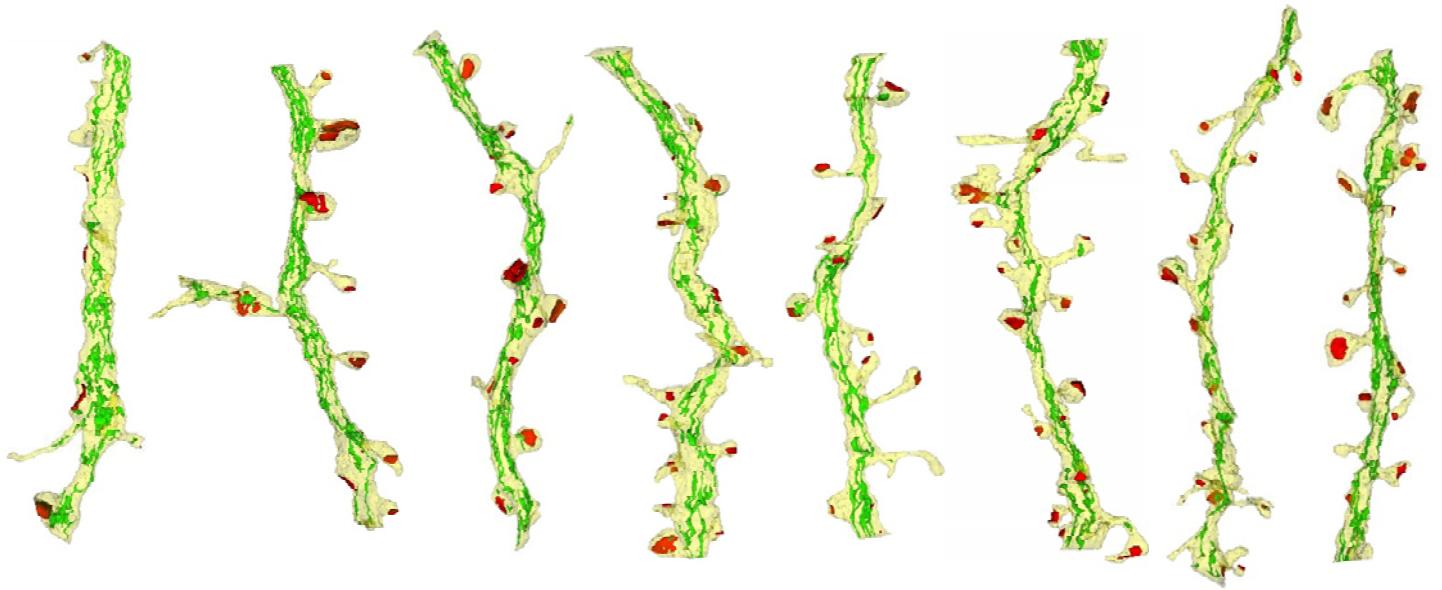
LTP
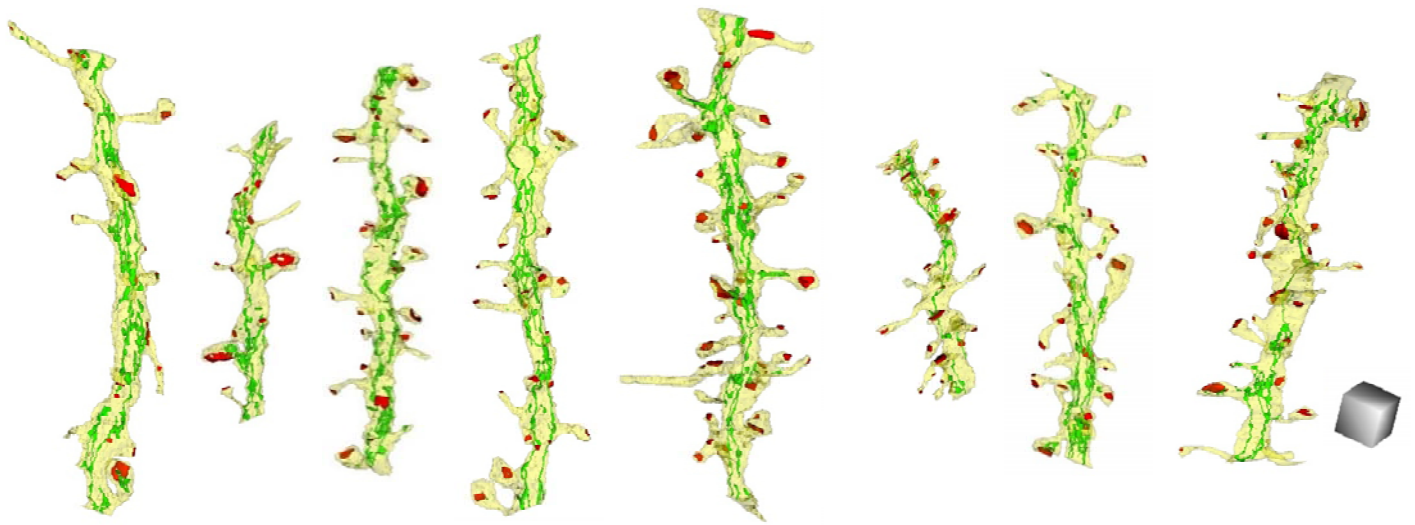
Figure 2 – figure supplement 1
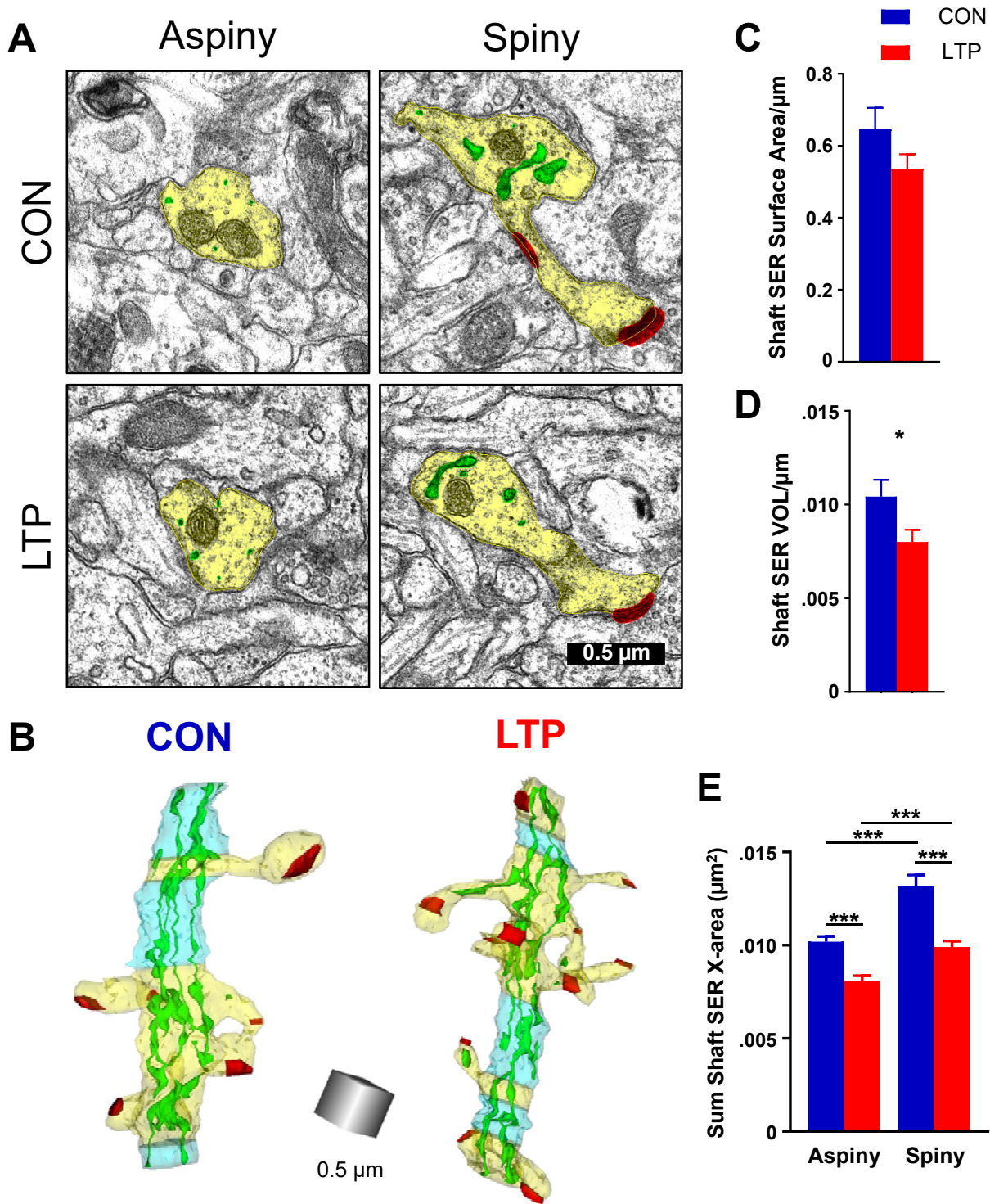
Figure 3
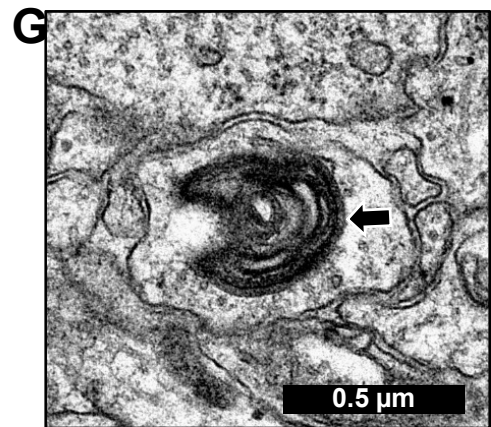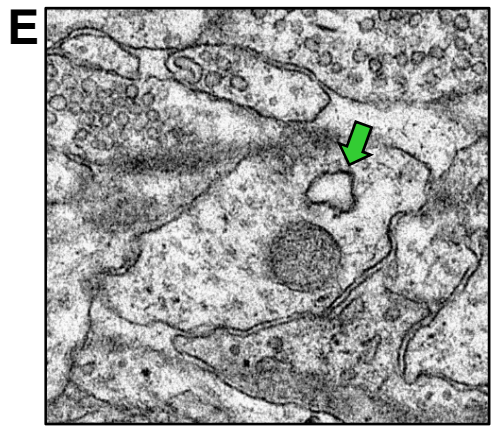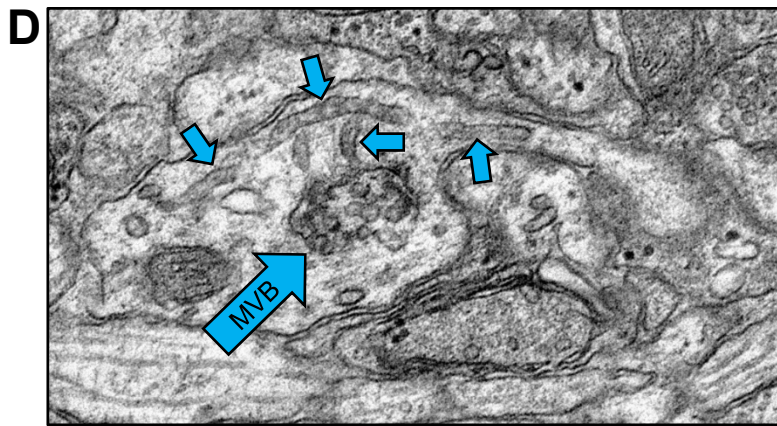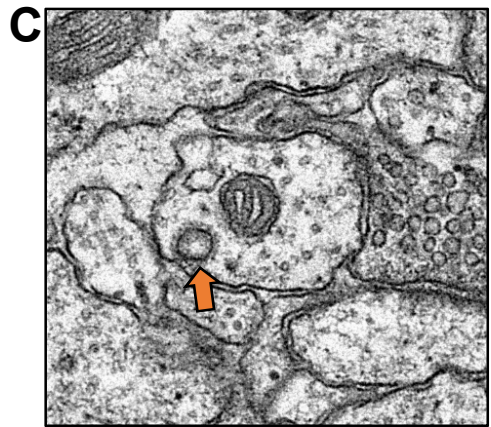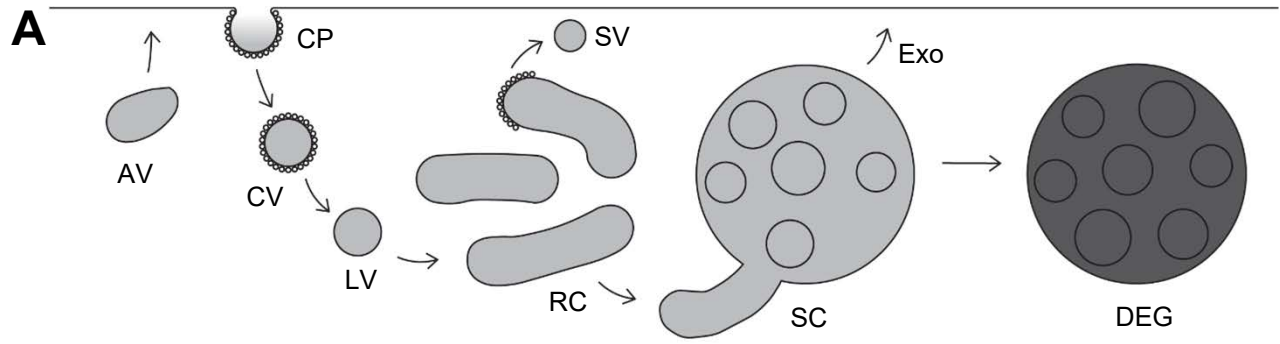
Figure 4
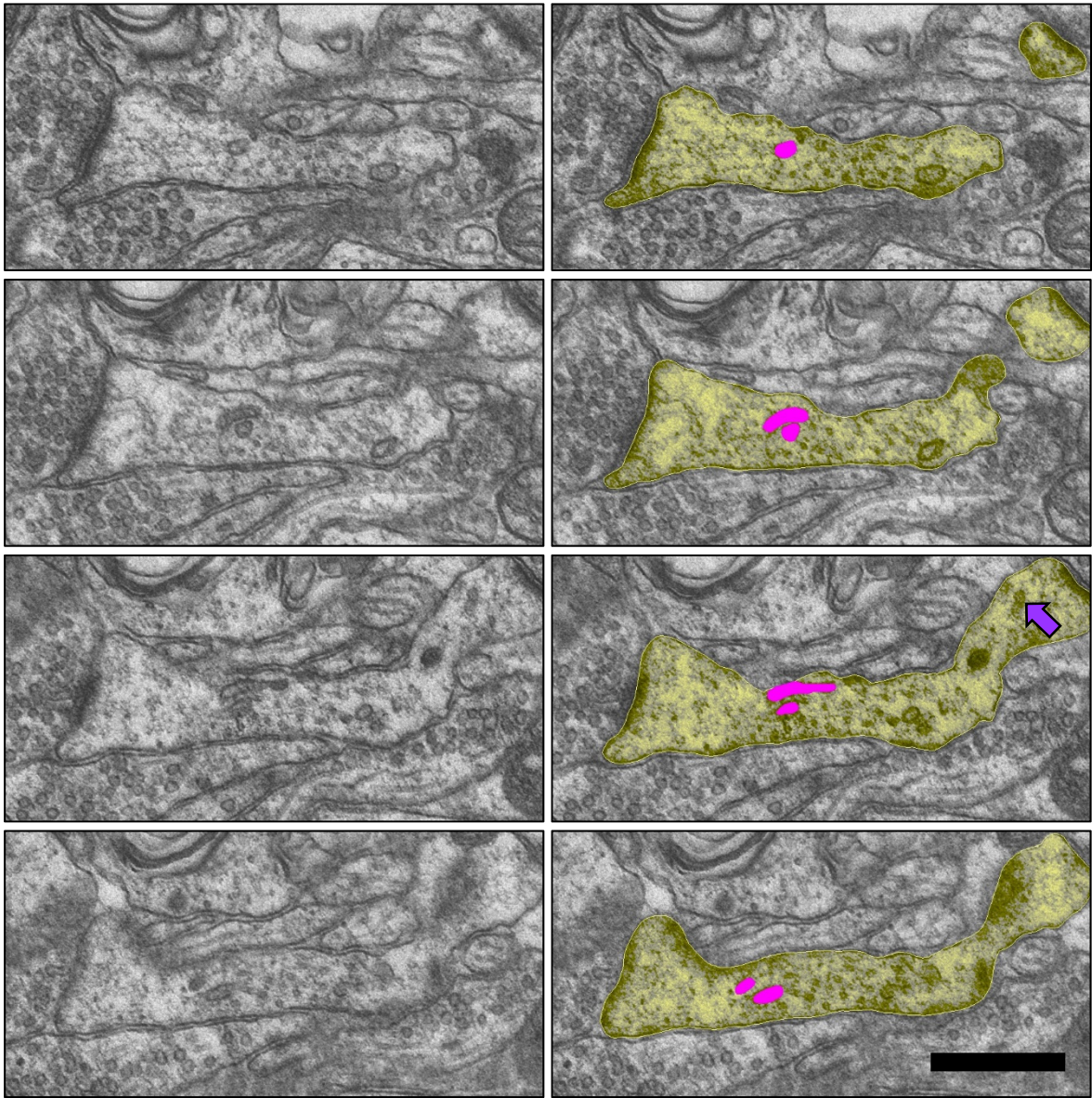
Figure 4 – figure supplement 1
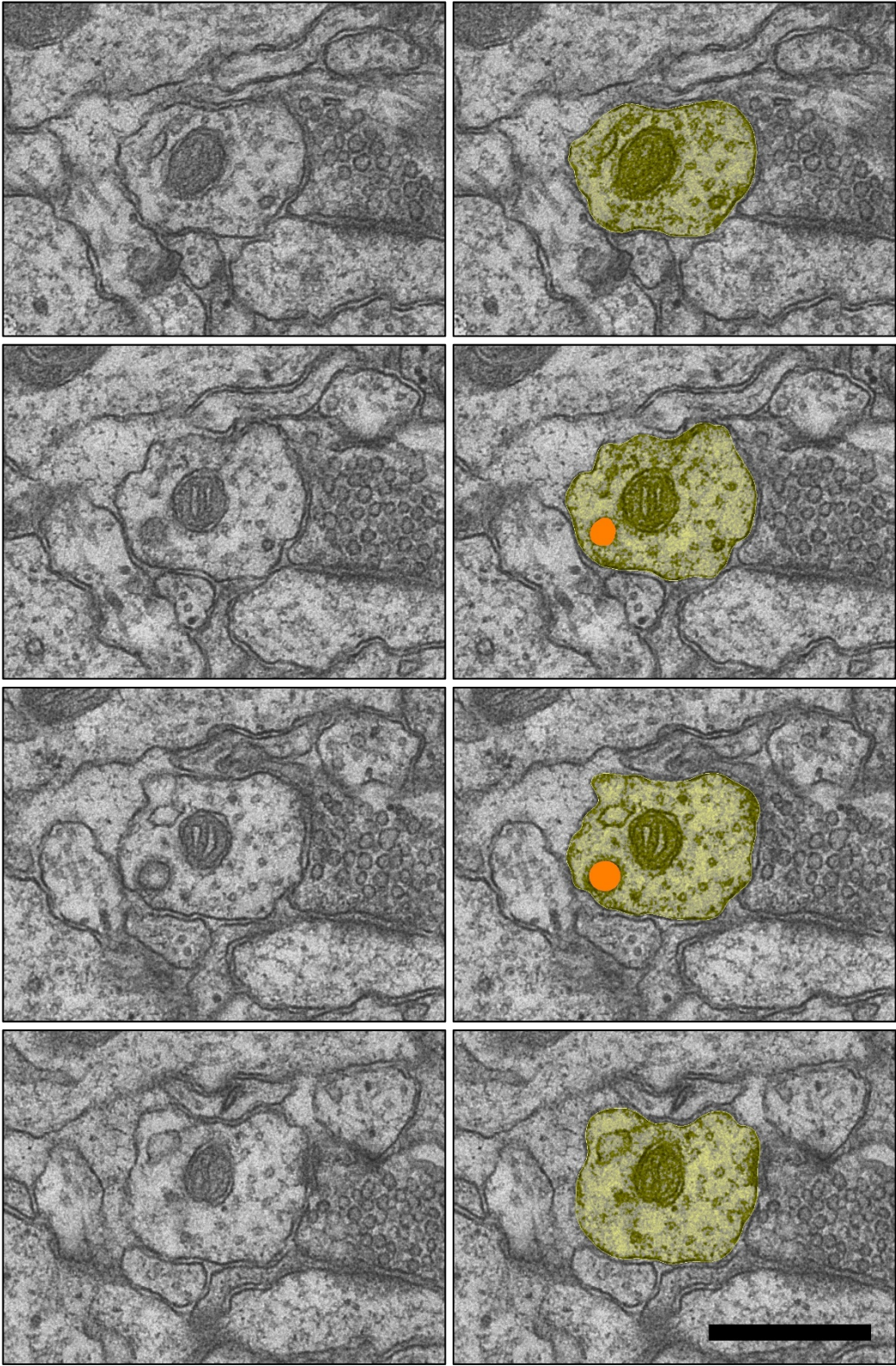
Figure 4 – figure supplement 2
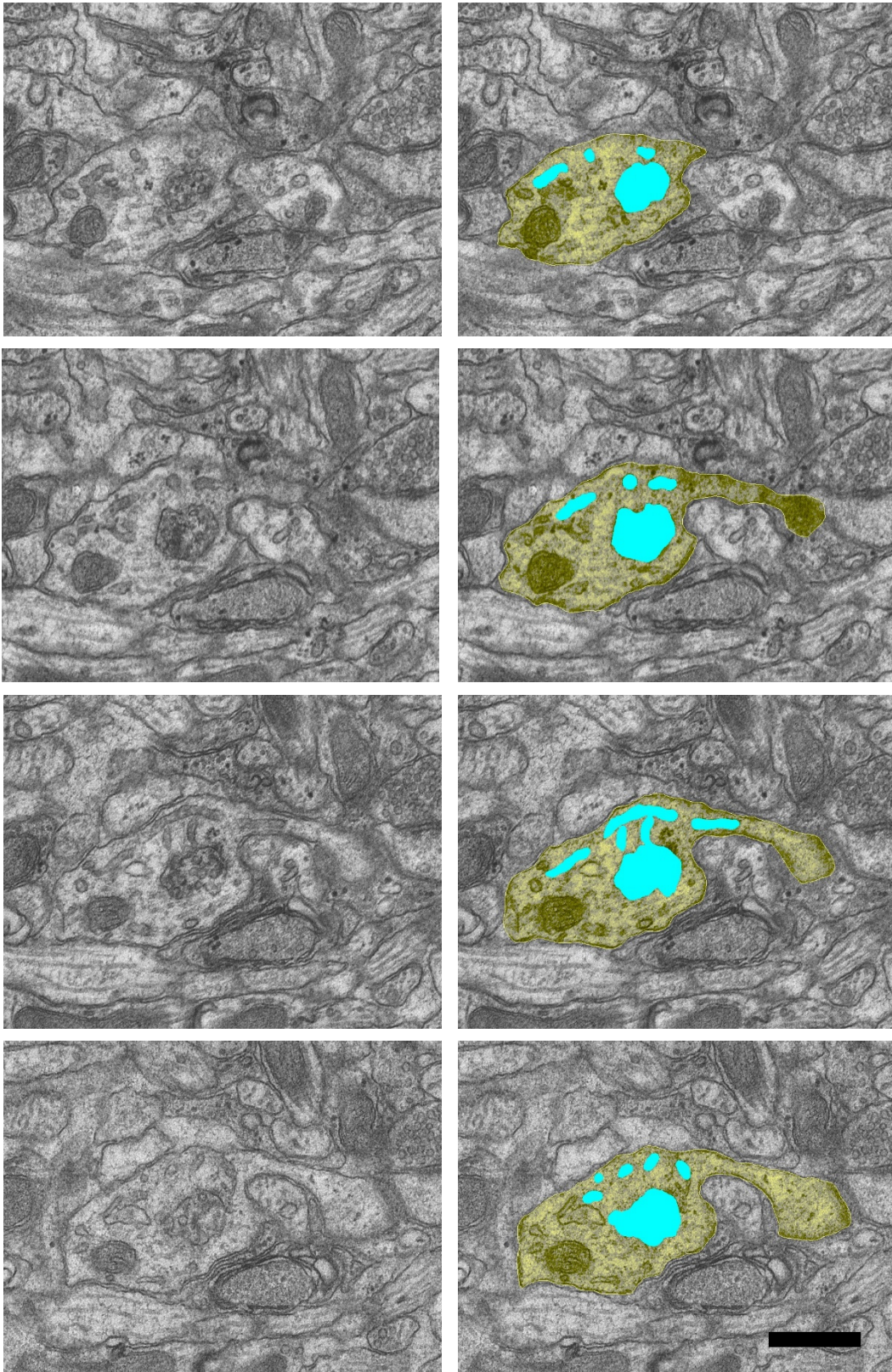
Figure 4 – figure supplement 3
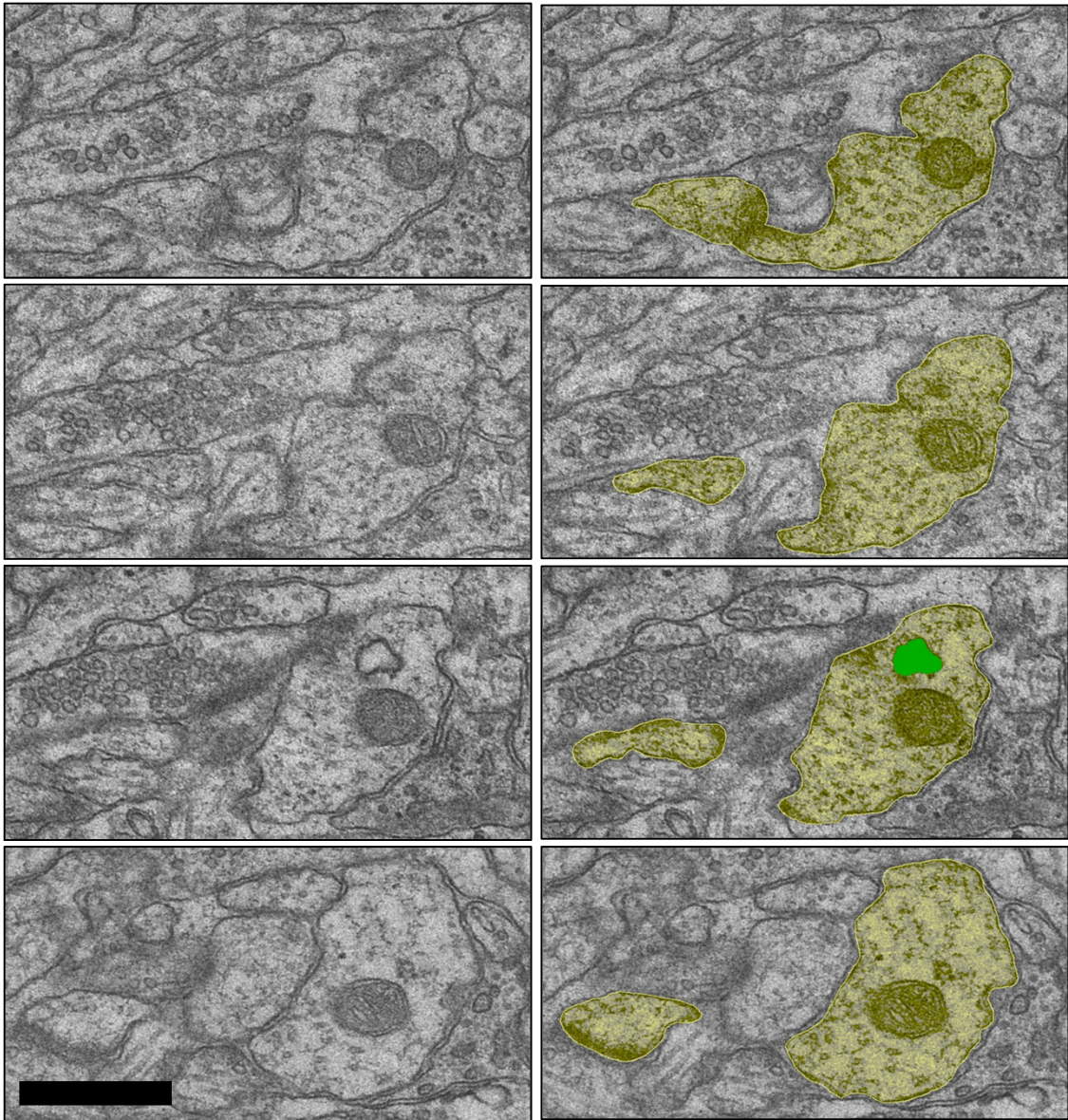
Figure 4 – figure supplement 4
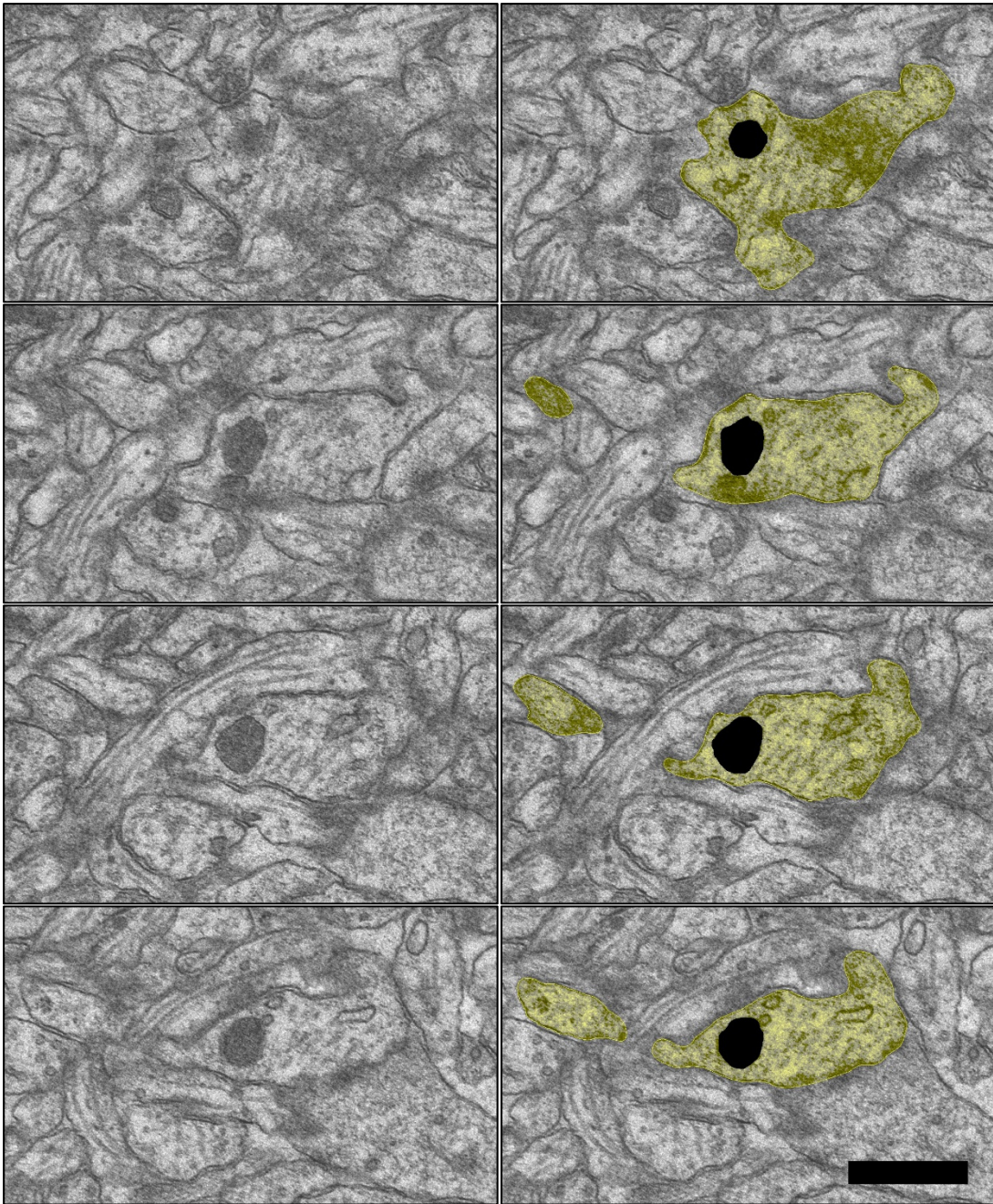
Figure 4 – figure supplement 5

Figure 4 – figure supplement 6

A

CON

0.5 μm

LTP

0.5 μm

1 μm³

● AV ● RC ● CP/CV/LV ● SC ● SV ● DEG

B **Dendritic Shaft**

Endosomes/μm

■ CON - Aspiny
■ CON - Spiny
■ LTP - Aspiny
■ LTP - Spiny

*

All Constr. AV CP/CV/LV RC SC SV Deg

C **Spines**

+Endo Sp / μm

■ CON
■ LTP

**
***

All PSD<0.05 PSD≥ 0.05

D

% +Endo Sp

E **PSD Area < 0.05 (μm²)**

Sp / μm

*

* *

*

All AV CP/CV/LV RC SC SV Deg
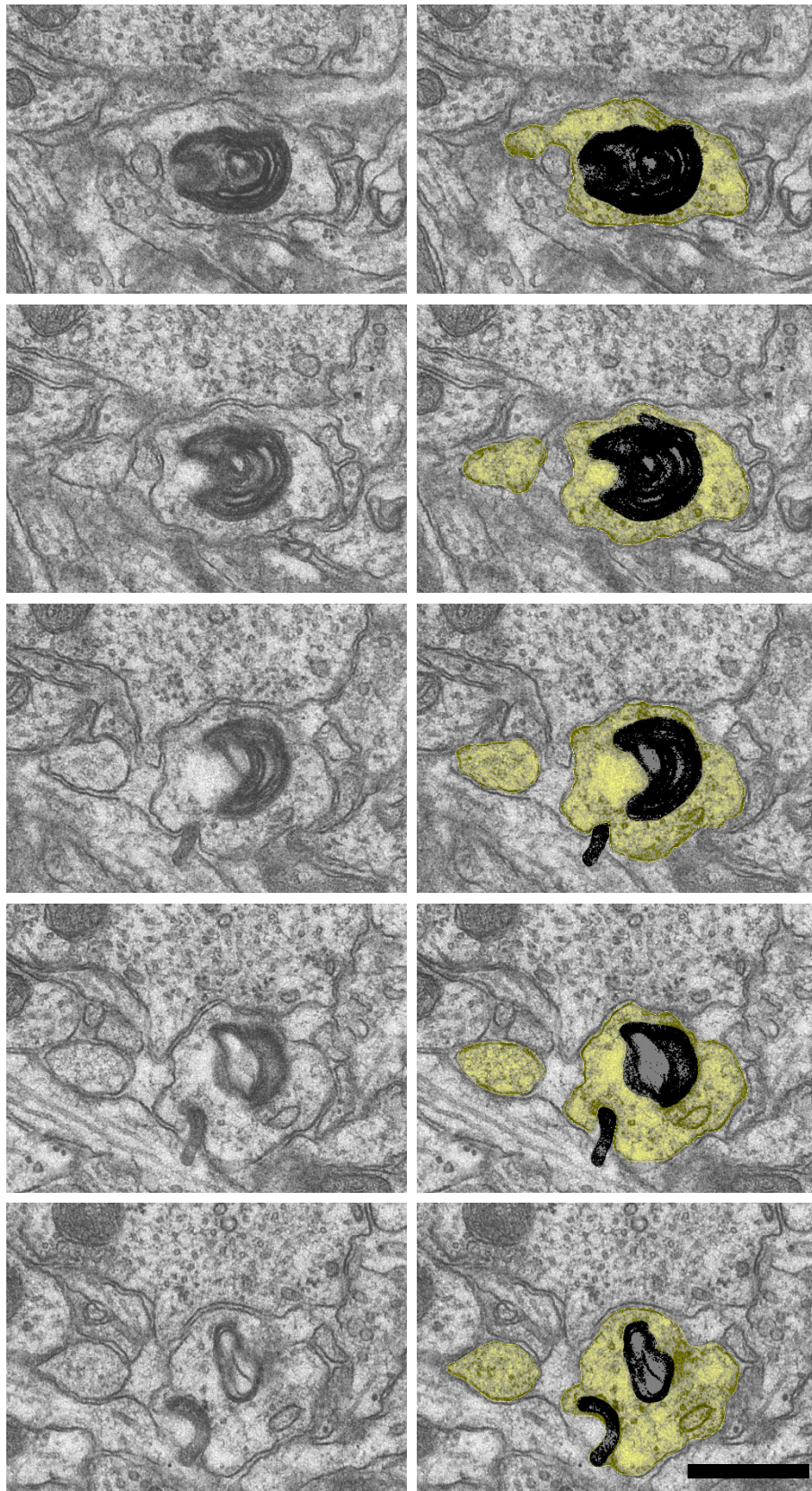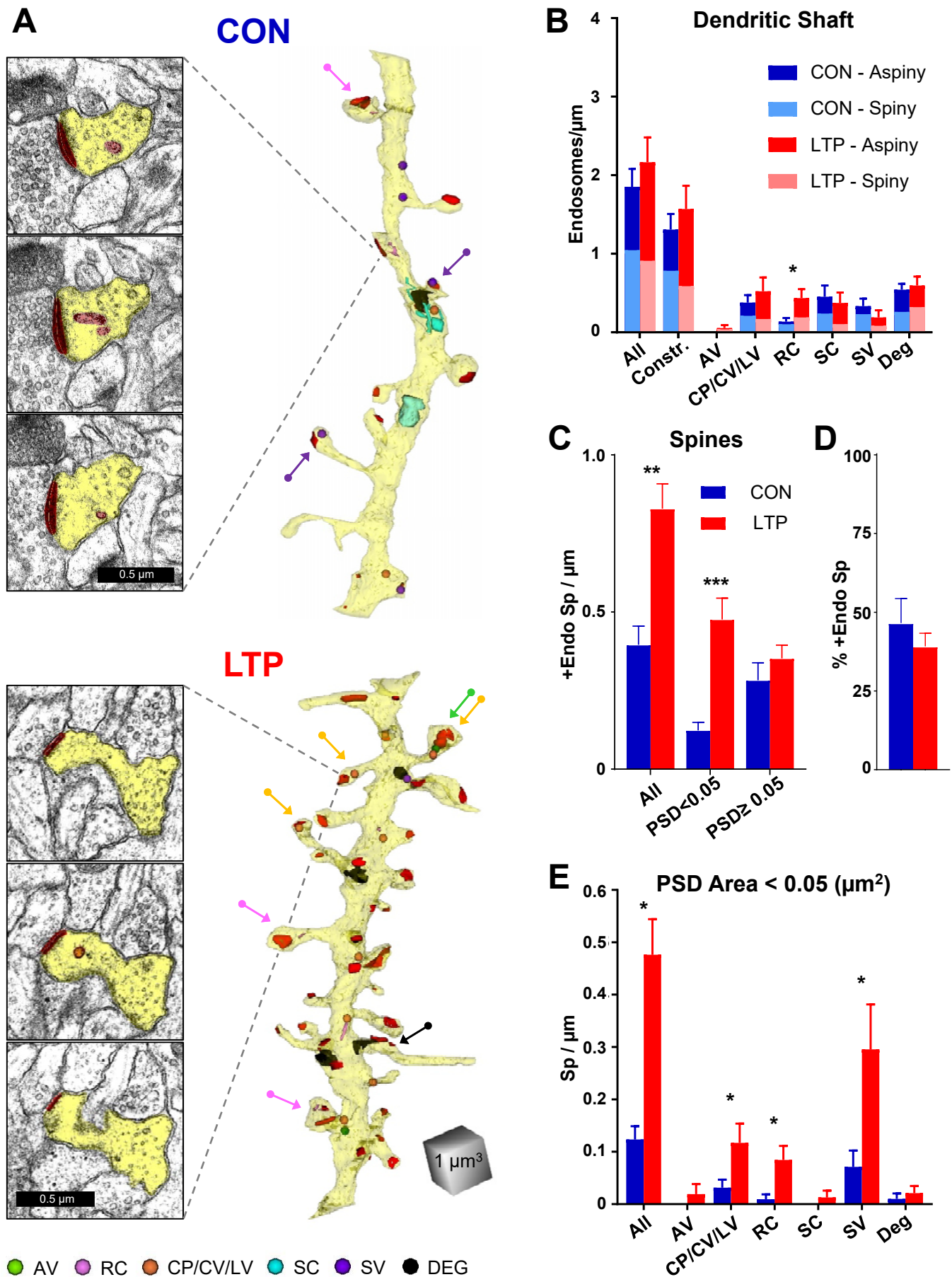
Figure 5

CON

LTP
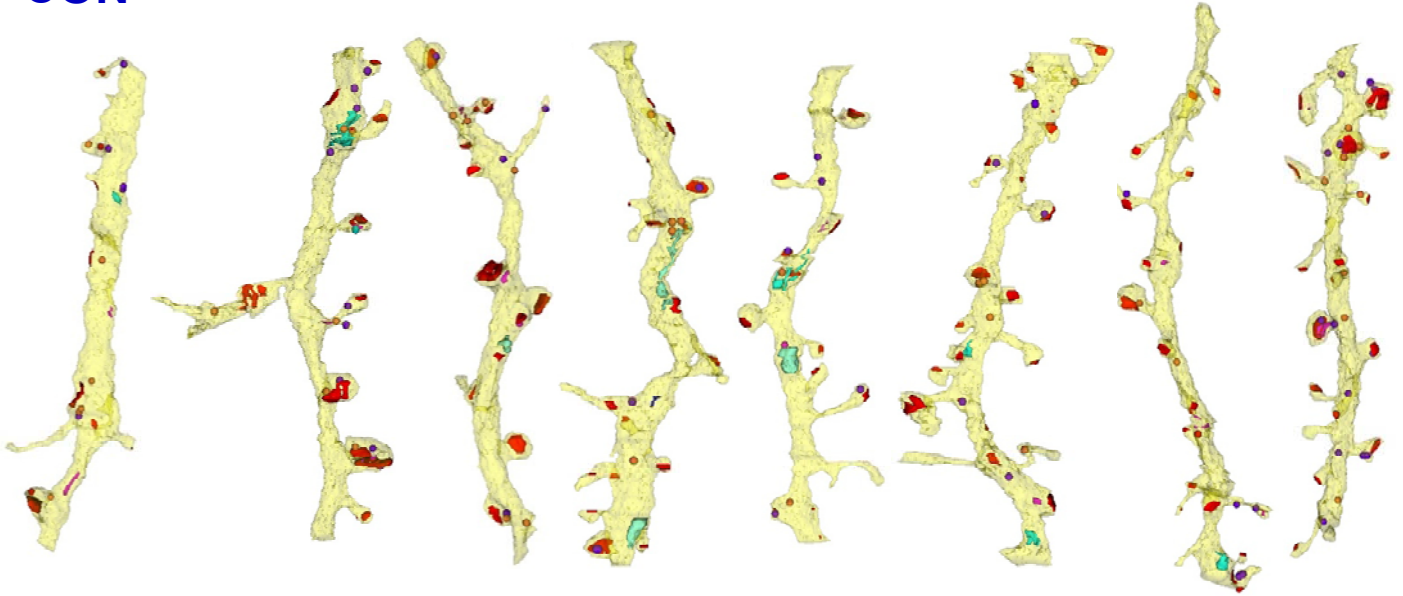
Figure 5 – figure supplement 1

CON

LTP

Figure 5 – figure supplement 2

Con   TBS ⟶ Early LTP ⟶ Late LTP

SER
PSD
RE
AMPAR

Figure 6